

NAVAL POSTGRADUATE SCHOOL  
Monterey, California



THESIS

ANALYSIS OF TEMPERATURE VARIABILITY BETWEEN  
DAVIDSON SEAMOUNT AND SUR RIDGE:  
THE TOMOGRAPHIC INVERSE PROBLEM

by

David O. Neander

June 2002

Thesis Advisor:  
Co-Advisor:

Ching-Sang Chiu  
Curtis A. Collins

Approved for public release; distribution is unlimited.

**REPORT DOCUMENTATION PAGE**Form Approved OMB No.  
0704-0188

Public reporting burden for this collection of information is estimated to average 1 hour per response, including the time for reviewing instruction, searching existing data sources, gathering and maintaining the data needed, and completing and reviewing the collection of information. Send comments regarding this burden estimate or any other aspect of this collection of information, including suggestions for reducing this burden, to Washington headquarters Services, Directorate for Information Operations and Reports, 1215 Jefferson Davis Highway, Suite 1204, Arlington, VA 22202-4302, and to the Office of Management and Budget, Paperwork Reduction Project (0704-0188) Washington DC 20503.

1. AGENCY USE ONLY (Leave blank)		2. REPORT DATE June 2002	3. REPORT TYPE AND DATES COVERED Master's Thesis	
4. TITLE AND SUBTITLE Analysis of Temperature Variability Between Davidson Seamount and Sur Ridge: The Tomographic Inverse Problem			5. FUNDING NUMBERS	
6. AUTHOR(S) David O. Neander			8. PERFORMING ORGANIZATION REPORT NUMBER	
7. PERFORMING ORGANIZATION NAME(S) AND ADDRESS(ES) Naval Postgraduate School Monterey, CA 93943-5000			10. SPONSORING/MONITORING AGENCY REPORT NUMBER	
9. SPONSORING / MONITORING AGENCY NAME(S) AND ADDRESS(ES)			10. SPONSORING/MONITORING AGENCY REPORT NUMBER	
11. SUPPLEMENTARY NOTES The views expressed in this thesis are those of the author and do not reflect the official policy or position of the U.S. Department of Defense or the U.S. Government.				
12a. DISTRIBUTION / AVAILABILITY STATEMENT Approved for public release; distribution is unlimited			12b. DISTRIBUTION CODE	
13. ABSTRACT (maximum 200 words)  As part of the Innovative Coastal-Ocean Observing Network (ICON), a receiver located on Sur Ridge monitored transmissions of low frequency tomography signals from a sound source on Davidson Seamount. The received signals were transmitted via underwater cable to the Point Sur Ocean Acoustics Observatory (OAO) from July 1998 through December 1999. Processed signals revealed a stable, resolvable arrival pattern. Subsequent analysis included forward acoustic modeling to calculate predicted raypaths. Observed arrivals were then associated with modeled raypaths, extracting observed travel times over the 17-month time series. Using a stochastic inverse approach, the extracted travel times were inverted for spatial and temporal variations of sound speed. Sound speed perturbation estimates were converted to temperature perturbations and compared to in situ mooring data, CTD transects along the acoustic path, and TOPEX/POSEIDEN satellite altimetry. Comparisons revealed that the tomographic estimate is in general agreement with the in situ point measurements and the altimeter data. The methods discussed in this paper demonstrate the application of ocean acoustic tomography to study temperature variability along the central California coast.				
14. SUBJECT TERMS Acoustic Tomography, Oceanography, Monterey Bay, ICON			15. NUMBER OF PAGES 59	
17. SECURITY CLASSIFICATION OF REPORT Unclassified			16. PRICE CODE	
18. SECURITY CLASSIFICATION OF THIS PAGE Unclassified		19. SECURITY CLASSIFICATION OF ABSTRACT Unclassified		20. LIMITATION OF ABSTRACT UL

NSN 7540-01-280-5500

Standard Form 298 (Rev. 2-89)  
Prescribed by ANSI Std. Z39-18

THIS PAGE INTENTIONALLY LEFT BLANK

Approved for public release; distribution is unlimited

**ANALYSIS OF TEMPERATURE VARIABILITY BETWEEN DAVIDSON  
SEMOUNT AND SUR RIDGE: THE TOMOGRAPHIC INVERSE PROBLEM**

David O. Neander  
Lieutenant Commander, National Oceanic and Atmospheric  
Administration  
B.S.M.E., University of California, Santa Barbara, 1986

Submitted in partial fulfillment of the  
requirements for the degree of

**MASTER OF SCIENCE IN PHYSICAL OCEANOGRAPHY**

from the

**NAVAL POSTGRADUATE SCHOOL  
June 2002**

Author:

David O. Neander

Approved by:

Ching-Sang Chiu, Thesis Advisor

Curtis A. Collins, Co-Advisor

Mary L. Batteen, Chairman  
Department of Oceanography

THIS PAGE INTENTIONALLY LEFT BLANK

## ABSTRACT

As part of the Innovative Coastal-Ocean Observing Network (ICON), a receiver located on Sur Ridge monitored transmissions of low frequency tomography signals from a sound source on Davidson Seamount. The received signals were transmitted via underwater cable to the Point Sur Ocean Acoustics Observatory (OAO) from July 1998 through December 1999. Processed signals revealed a stable, resolvable arrival pattern. Subsequent analysis included forward acoustic modeling to calculate predicted raypaths. Observed arrivals were then associated with modeled raypaths, extracting observed travel times over the 17-month time series. Using a stochastic inverse approach, the extracted travel times were inverted for spatial and temporal variations of sound speed. Sound speed perturbation estimates were converted to temperature perturbations and compared to in situ mooring data, CTD transects along the acoustic path, and TOPEX/POSEIDEN satellite altimetry. Comparisons revealed that the tomographic estimate is in general agreement with the in situ point measurements and the altimeter data. The methods discussed in this paper demonstrate the application of ocean acoustic tomography to study temperature variability along the central California coast.

THIS PAGE INTENTIONALLY LEFT BLANK

## TABLE OF CONTENTS

I. INTRODUCTION.....	1
A. PHYSICAL OCEANOGRAPHY OF CENTRAL CALIFORNIA.....	1
B. THE INNOVATIVE COASTAL-OCEAN OBSERVING NETWORK.....	3
C. OCEAN ACOUSTIC TOMOGRAPHY.....	4
D. THESIS OBJECTIVES AND APPROACH.....	7
E. THESIS OUTLINE.....	8
II. OBSERVATIONS.....	9
A. ACOUSTIC TOMOGRAPHY.....	9
1. The Experiment.....	9
2. Signal Characteristics.....	12
3. Arrival Structure.....	14
B. OCEANOGRAPHIC DATA.....	17
1. Shipboard Data.....	17
2. Moored Temperature Data.....	18
III. FORWARD MODELING.....	21
A. HAMILTONIAN RAY TRACING.....	21
B. ARRIVAL STRUCTURE.....	22
C. RAY IDENTIFICATION.....	26
D. TRAVEL TIME VARIABILITY.....	30
IV. TOMOGRAPHIC INVERSE.....	33
A. DEVELOPMENT OF THE INVERSE PROBLEM.....	33
B. VERTICAL STRUCTURE AND CONSTRAINT.....	34
C. INVERSION.....	37
D. RESULTS AND DISCUSSION.....	38
1. Resolution and Mean Square Error of the Tomographic Estimate.....	38
2. Interpretation of Tomographic Estimate.....	40
3. Comparison to Moored Temperature Data.....	43
4. Comparison to CTD Transects.....	45
5. Comparison to TOPEX/POSEIDEN Altimetry.....	51
V. CONCLUSIONS.....	53
LIST OF REFERENCES.....	55
INITIAL DISTRIBUTION LIST.....	59

THIS PAGE INTENTIONALLY LEFT BLANK

## ACKNOWLEDGMENTS

I would like to take this opportunity to thank my thesis advisor, Professor Ching-Sang Chiu for his guidance, insight and stimulation in the subject. Ching-Sang provided me with the necessary tools to complete the project, helped me solve numerous programming errors, and gave me often-needed reality checks.

I would like to thank Professor Curtis Collins for his seemingly endless supply of oceanographic data, as well as his expertise in the oceanography of the Central California coast.

I would also like to thank Dr. John Ryan of the Monterey Bay Aquarium Research Institute for providing me with TOPEX/POSEIDEN satellite altimetry data.

I would like to extend special thanks to Chris Miller, who provided much needed insight and answered my numerous questions on tomography, data analysis and signal processing. Without Chris's assistance, I would still be signal processing.

Finally, I would like to thank my wife Julia and son Forrest for their patience and support over my two years at NPS.

THIS PAGE INTENTIONALLY LEFT BLANK

## I. INTRODUCTION

### A. PHYSICAL OCEANOGRAPHY OF CENTRAL CALIFORNIA

The California coast is an oceanographically complex region, little understood and inadequately sampled. Increased understanding of the features and dynamics of this region can aid fisheries and wildlife management, prediction and abatement of pollution and toxic phytoplankton blooms, atmospheric and climate change forecasts, and shipping and military operations (Miller, 1999)

Large-scale atmospheric forcing in the eastern Pacific Ocean consists of the North Pacific High, the Aleutian Low, and in summer the thermal low over the western United States. The North Pacific High is most intense during the summer months while the Aleutian Low is most intense during the winter months. During summer months, interaction between the North Pacific High and the thermal trough inland helps to strengthen and expand the northerly surface winds along the west coast of the California. This forcing contributes to the creation of the anticyclonic North Pacific Subtropical Gyre. The California Current System (CCS) forms the eastern limb of this gyre, flowing equatorward from Washington to Baja California. The CCS has traditionally been divided into three large-scale (> 500 km) alongshore currents: the California Current (CC), the Davidson Current (DC), and the California Undercurrent (CUC) (Hickey, 1998).

The CC is a surface (0-300 m deep) current, which carries colder, fresher subarctic water equatorward

throughout the year with average speeds generally less than  $25 \text{ cm s}^{-1}$  (Reid and Schwartzlose, 1962). Thus, the CC is characterized by a low salinity, low temperature core which usually lies between 300-400 km offshore (Lynn and Simpson, 1987). The CUC flows poleward over the continental slope from Baja to at least  $50^\circ \text{ N}$  with a relatively narrow width between 10-40 km (Hickey, 1998). The CUC has its origin in the eastern equatorial Pacific, and is identified by its warm, saline, oxygen and nutrient-poor signature. Hickey (1979) concluded that the location, strength and core depth show considerable seasonal variability and can be related to the seasonal variability in wind stress and curl of the wind stress. Peak speeds of the undercurrent are about  $30\text{-}50 \text{ cm s}^{-1}$ , being stronger at depths of 100-300 m, and can be continuous over distances of more than 400 km along the slope (Collins *et al.*, 1996). The DC is a seasonal current, flowing poleward at the surface during the fall and winter over the shelf from Point Conception to Vancouver Island. Measurements in the region have shown that the seasonal cycle over the slope is highly variable with the poleward flow maximum usually occurring in May (Collins *et al.*, 1996). The reversal of winds from northwesterly in summer to southeasterly in winter, which causes downwelling at the coast, seems to be the forcing mechanism of this poleward surface current (Huyer *et al.*, 1989). It has been suggested that the DC is a result of the "surfacing" of the CUC during late fall (Pavlova, 1966; Huyer and Smith, 1974).

The Central California Coast, particularly in the vicinity of Monterey Bay, has the added complexity of highly variable bathymetry, which influences currents that

make up the CCS. This oceanographically complex region, which consists of variable currents, mesoscale eddies and upwelling events, exhibits significant variability from synoptic to interannual scales. It became apparent that a long-term, near real-time coastal observing network was needed to collect information on critical ocean parameters, for input into predictive models for the purpose of forecasting coastal ocean conditions.

#### **B. THE INNOVATIVE COASTAL-OCEAN OBSERVING NETWORK**

Funded by the National Ocean Partnership Program (NOPP), an alliance was formed between government, academic, and industrial entities to implement an Innovative Coastal-Ocean Observing Network (ICON) to study the oceanography in the Central California Coastal waters surrounding Monterey Bay (Paduan *et al.*, 1999). The partnership involves a consortium of scientists and engineers from eight organizations, including the Naval Postgraduate School (NPS), Monterey Bay Aquarium Research Institute (MBARI), California State University at Monterey Bay (CSUMB), University of Southern Mississippi (USM), University of Michigan (UM), HOBI Labs, CODAR Ocean Sensors Ltd. (COS), and the Naval Research Laboratory (NRL). The goals of ICON were to bring together modern measurement technologies, to develop new technologies, and to integrate them within a data-assimilating coastal ocean circulation model.

The principal components of the observing network include 1) surface current maps from shore-based high frequency (HF) radar installations, 2) subsurface currents,

temperature, salinity and bio-optical properties plus surface meteorological properties from several deep-sea moorings, 3) sea surface temperature and color from satellites, and 4) along-track temperature and temperature variances from two acoustic tomography slices through the region.

The acoustic tomography component consists of two autonomous sound sources, one placed on Davidson Seamount and the other on Pioneer Seamount. These seamounts allowed for the placement of transmitters near the sound channel axis. In addition, the transmitter would be in close proximity to the bottom, which keeps mooring motion within tolerable limits. A receiver located on Sur Ridge monitored the acoustic transmissions from these two sources continuously. The data were transmitted real time via underwater cable to the NPS Ocean Acoustic Observatory (OAO) facility at Point Sur.

### **C. OCEAN ACOUSTIC TOMOGRAPHY**

Ocean acoustic tomography is a technique for observing the dynamic behavior of ocean processes by measuring the changes in travel time of acoustic signals transmitted over a number of ocean paths (Spindel, 1986). The word tomography is derived from the two Greek roots meaning "to slice" and "to look at." Tomography is an imaging technique that inverts propagation measurements through many sections of a volume to determine the physical characteristics of the interior of the volume (Medwin and Clay, 1998). Analogous techniques are employed in medical tomography (e.g., X-rays in Computer Assisted Tomography

(CAT) scans) or geophysical tomography, which uses manmade shock waves to explore the earth's interior. Munk and Wunsch (1979) first proposed application of these techniques to the ocean as a means for monitoring ocean basins for mesoscale fluctuations. Ocean acoustic tomography uses sound energy to "look at" a "slice" of the ocean by measuring the travel times of various signals propagating along different acoustical paths through the volume. As acoustic energy travels along its path, sound speed fluctuations affect the travel time. Since sound speed in the ocean is a function of temperature, salinity and pressure, information is acquired about these parameters as well as current speeds and direction. These data are in the form of sound pulse travel time changes. Using these measurements of travel time perturbations, an estimate of the ocean structure can be constructed using mathematical inverse techniques.

Ocean acoustic tomography has several advantages over more traditional oceanographic study methods (Chiu *et al.*, 1987). An acoustic tomography system can be installed in the ocean as a semi-permanent, continuous, weather-independent observing system. The low spatial attenuation rate of sound and high temporal resolution allows the system to monitor large volumes of the ocean interior, sampling many different levels simultaneously. Since relatively few acoustic moorings are required for ocean acoustic tomography, costs associated with such a system are significantly lower than conventional "spot" mooring systems. Furthermore, with each additional conventional mooring only one piece of information is added such that a 1:1 mooring increase to information-gain ratio occurs. In

contrast, the addition of one tomographic mooring adds many new distinct ray paths, each of which adds a piece of information to the system (Munk and Wunsch, 1979).

The applicability of acoustic tomography for monitoring ocean variability is dependent upon the following four important issues: 1) stability, 2) resolvability, 3) identifiability, and 4) signal-to-noise ratio (SNR). Stability addresses the property of whether or not the same individual arrival exists over successive transmissions. Stability requires transmitter-receiver paths to be insensitive to changes and not fade away or disappear. These transmitter-receiver paths are called eigenrays. Resolvability requires that the arrival time separation between eigenrays be sufficient to resolve individual rays. The third issue, identifiability, requires that measured arrival times of eigenrays correspond to modeled arrival times, thus associating arrivals to raypaths. Lastly, adequate signal-to-noise ratios are required to ensure travel time precision, and that the signals are strong enough to be received over background noise.

An ocean acoustic tomography experiment can be divided into two separate and distinct parts. The first is the forward problem, which establishes the physical relationship between the data and the unknown structure given the characteristics of the sound channel and sensor configuration. The second is the inverse problem, which demands calculation of the unknown ocean perturbations given raypath geometries and travel time measurements.

#### D. THESIS OBJECTIVES AND APPROACH

The principal objective of this thesis is to study the temperature variability along the California coast between Davidson Seamount and Sur Ridge during the period from 30 July 1998 to 31 December 1999. During this timeframe, the sound source at Davidson Seamount emitted tomographic signals continuously, with the exception of intermittent data gaps. Although the data gaps preclude the analysis of fast temperature fluctuations, the overall time series allows for an adequate analysis of mesoscale variability. In conjunction with mooring temperature data in the vicinity of the acoustic path, the Davidson Seamount to Point Sur transmission has allowed for an in-depth evaluation of the feasibility of using acoustic tomography in monitoring the coastal environment for mesoscale fluctuations.

The analysis of the tomographic data has been divided into three distinct areas:

1. Forward Modeling. Acoustic propagation modeling was first conducted to examine the expected ray arrival structure. The acoustic modeling uses a ray theory approach, which incorporates a reference or "background" sound speed profile derived from data acquired in July 1998 by the R.V. POINT SUR and a high resolution bathymetric dataset obtained from the National Oceanic and Atmospheric Administration (NOAA). To validate the model results, predicted arrivals were compared to observed arrivals, associating the observed arrivals with the predicted eigenrays.

2. Time Series Construction. Travel times for stable and strong ray arrivals were extracted from the time series data. A 7<sup>th</sup>-order polynomial was used to interpolate through data gaps and smooth edge effects, while a 4<sup>th</sup>-order, 10-day low-pass filter was used to filter out fast fluctuations such as tidal oscillations.

3. Inverse Analysis. The time series of ray travel times were then "inverted" using a minimum mean-square error estimator. The temporal and horizontal structure of temperature along the acoustic path was estimated by constraining the vertical structure using a 3-layer model approach. Validation of the tomographic inverse and interpretation of the oceanographic variability were aided by mooring temperature data, CTD transects and TOPEX/POSEIDEN satellite altimetry.

#### **E. THESIS OUTLINE**

The remainder of this thesis consists of four additional chapters. Chapter II includes a discussion of acoustic tomography and oceanographic measurements as they pertain to this thesis. Chapter III presents and discusses forward modeling results, the extracted time series of ray travel times and ray identification. Chapter IV presents the vertical structure and constraint of the tomographic estimate, discusses development and results of the inverse problem, and compares the observed acoustic variability in relation to observed oceanographic processes. Conclusions are presented in Chapter V.

## II. OBSERVATIONS

### A. ACOUSTIC TOMOGRAPHY

#### 1. The Experiment

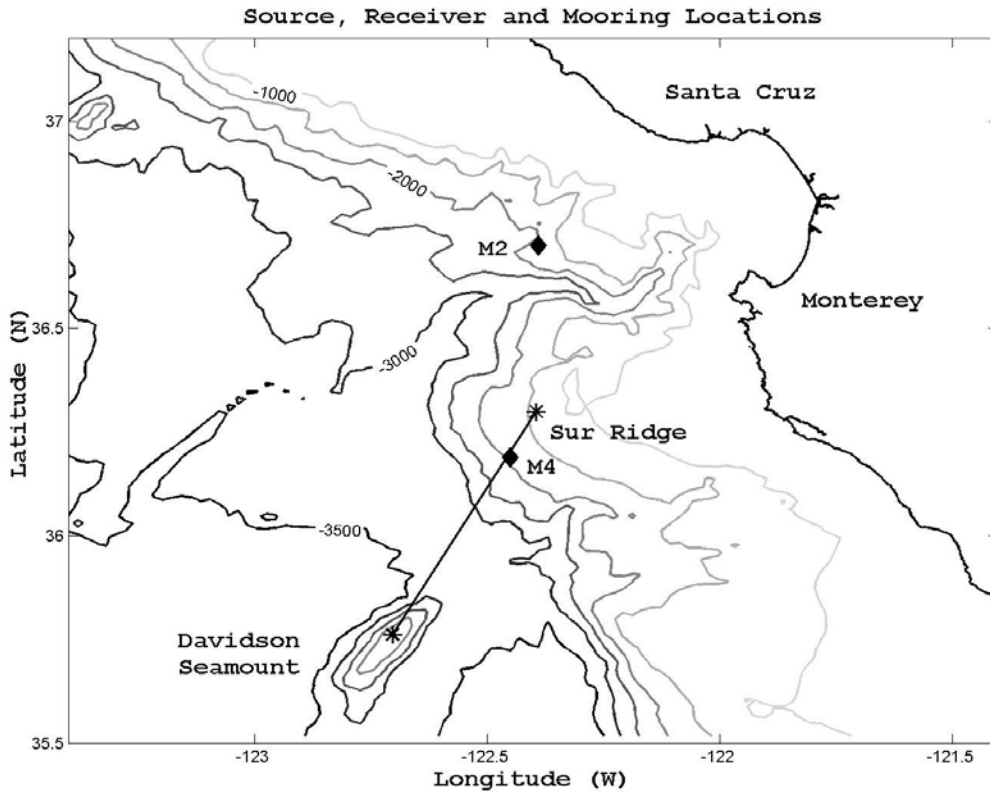


**Figure 1 - Contour map depicting the orientation of the tomography source and receiver**

The tomography experiment extended from a transmitter located on Davidson Seamount northeast to a receiver placed on Sur Ridge. This region and location of the transmitter and receiver are shown in Figure 1. The transmitter and receiver were located at depths of 1270 and 1359 m, respectively. The transmitter produced phase-modulated signals, with a source level of 180 dB re  $1\mu\text{Pa}$ , center

frequency of 400 Hz, and bandwidth of 100 Hz. The tomographic signals recorded at Sur Ridge were transmitted via underwater cable to the NPS Point Sur OAO. Transmissions were recorded from July 1998 through December 1999. Figure 2 depicts a vertical cross-section of the bathymetry along the 66-km acoustic path. The bathymetry was interpolated from a high-resolution digital dataset extracted using GEODAS (GEOphysical DATA System), an interactive database management system obtained from the NOAA National Geophysical Data Center (NGDC).

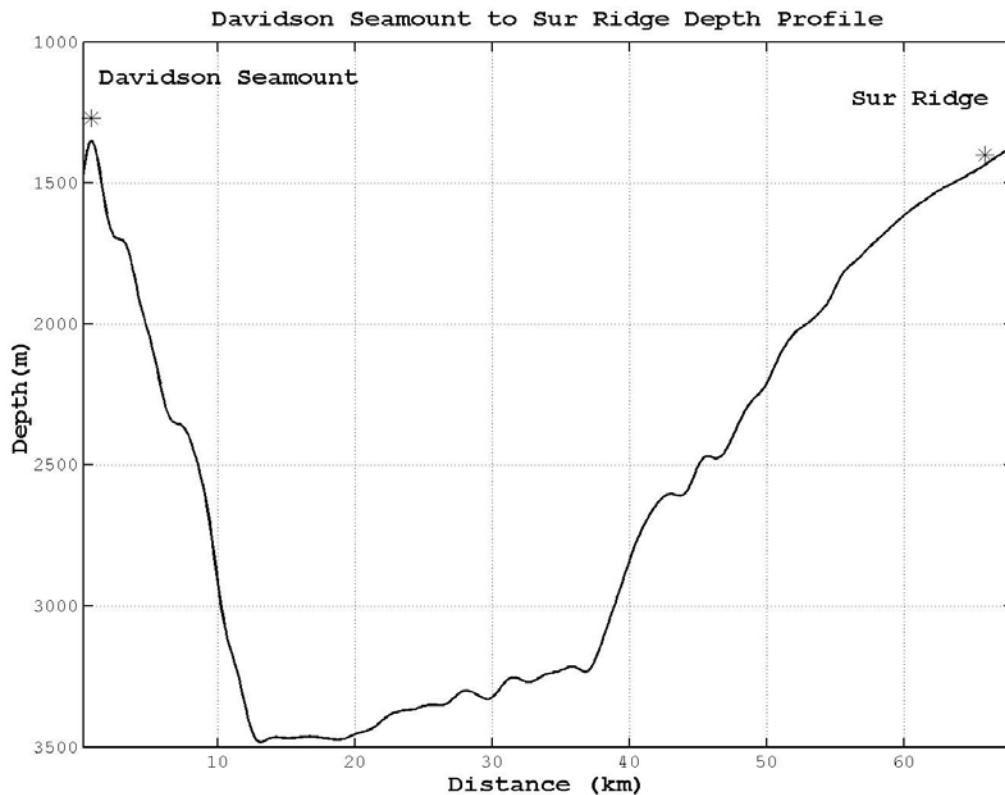


**Figure 2 - Davidson Seamount to Sur Ridge Bathymetry**

In a bottom-limited configuration, ray propagation becomes more complex as rays interact with the bottom. Complicated multipath arrivals or "micro-multipaths" may

reach the receiver simultaneously, which exacerbates the problem of identifying individual observed arrivals with modeled ray paths. Figure 3 offers a three-dimensional view of the source-receiver configuration with associated bathymetry and example eigenray paths.

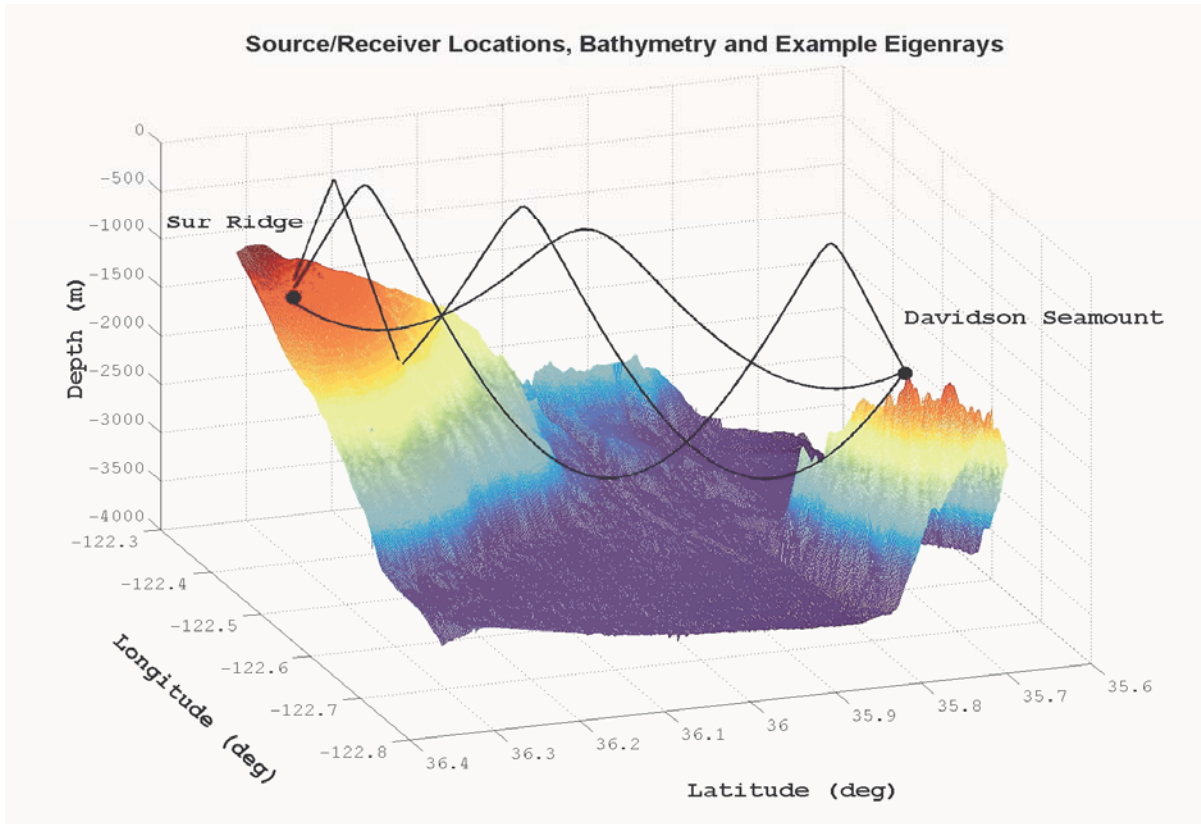


**Figure 3 - Sample eigenrays, Davidson Seamount source, and Sur Ridge receiver**

During the course of data acquisition, numerous outages at the NPS Point Sur OAO resulted in data gaps in the travel time series. Significant outages (> 2 days) are summarized in Table 1.

Data Outage (year/day)	Length (hrs)	Reason for Outage
1998 226-231	119.3	loss of building power
1998 318-321	49.1	disk storage 100% full
1999 012-147	3239.1	time synchronization lost
1999 147-167	498	time synchronization errors
1999 251-297	1104.55	power transformer damaged
1999 338-344	159.48	power outage - blown breaker
2000 001		all transmissions stop
Length of all outages: 5356.04 hrs		
Percent of study period: 43.06%		

Table 1 - Significant outages affecting data continuity

## 2. Signal Characteristics

The traditional approach to signal design and processing in ocean acoustic tomography is that described by Birdsall and Metzger, 1986. Their method exploits phase modulation of the periodic signals using maximal length (binary) sequences (m-sequences) to achieve optimal pulse compression with no side lobes. Modulating the signal's phase with an m-sequence and processing with a correlation-matched filter results in a deterministic narrow pulse, which leads to a signal processing gain of  $10\log(511)$  (where 511 is the m-sequence length). Transmitting this sequence repeatedly leads to additional signal processing gain of  $10\log(35)$  at the receiver by coherently averaging

the consecutive sequences (35 m-sequences transmitted). Source signal characteristics are summarized in Table 2.

<b>Source Characteristics - Davidson Seamount</b>	
<b>Source level</b>	<b>180 dB re 1<math>\mu</math>PA at 1 m</b>
<b>Center frequency</b>	<b>400 Hz</b>
<b>Full bandwidth</b>	<b>100 Hz</b>
<b>m-sequence law (octal)</b>	<b>1021</b>
<b>m-sequence length</b>	<b>511 digits (signal processing gain of 27 dB)</b>
<b>Digital width (resolution)</b>	<b>4 cycles = 10 msec</b>
<b>m-sequence period</b>	<b>5.11 sec</b>
<b>m-sequences transmitted</b>	<b>35 sequences (signal processing gain of 15 dB)</b>
<b>Transmission length</b>	<b>178.85 sec</b>

**Table 2 - Characteristics of the 400 Hz tomography signal**

The sound source was programmed to transmit signals at two different rates, for the purpose of resolving oceanographic variability. From 30 July to 28 August 1998 the source transmitted every 30 minutes, the objective being to resolve high-frequency oscillations such as internal tides. From 28 August 1998 thereafter, the source transmitted every 12 hours to resolve longer-term variations. At the Point Sur OAO, two different sampling rates were utilized. A sampling rate of 1000 Hz was initially utilized. Even though this sampling rate met the Nyquist criterion, it proved insufficient to produce an improved SNR through coherent averaging of multiple arrival structures. The sampling rate was changed to 2000 Hz on 29

August 1998 and continued at this rate through December 1999.

One of the fundamental issues in ocean acoustic tomography is the ability to record time accurately. A SeaScan temperature-compensated quartz crystal clock provided timing control at the source. The receiver used a GPS trigger to start data acquisition, with a crystal oscillator determining the sample rate. Significant rate variability was observed after power outages. This led to the calculation of drift rates, which are summarized in Table 3 along with additional timing inconsistencies determined during the July 1998 to December 1999 time series.

Timing Error	Data Set	Correction
Clock offset	Entire time series	-0.098307 sec
File-by-file drift	1998-1000 Hz	+0.4548 sec/day
File-by-file drift	1998-2000 Hz (242-317)	+0.4619 sec/day
File-by-file drift	1998-2000 Hz (318-365)	+0.3629 sec/day
File-by-file drift	1999-2000 Hz	+0.4012 sec/day
Source drift	Entire time series	+0.00126 sec/day
Leap Second	1999-2000 Hz	+1.0 sec

Table 3 - Timing Corrections

### 3. Arrival Structure

A correlation-matched filter was applied to the data, with the output corresponding to a sum of pulses arriving

from the multiple eigenray paths. An improved signal-to-noise ratio was obtained through coherent averaging. Each transmission was processed and inspected individually. Figure 4 depicts a typical arrival pattern of one transmission while Figure 5 shows an example waterfall plot of transmissions from 30 July 1998 to 12 January 1999. The waterfall plot is useful for examination of arrival stability, and assists in determination of whether the arrival peaks are resolvable over the entire time series.

Once all transmissions were processed, the travel times of the arrival peaks were extracted. Travel times within a window were picked for peaks that exceeded a median amplitude threshold value for that window. Since the time series covered over 17 months, the travel time of an individual arrival can change more than the separation between individual arrivals. This led to using multiple windows and adjusting the window accordingly to keep the arrival time peaks within the limits of the window. Applying a 7th-order polynomial to fill in small data gaps and smooth edge effects further refined the arrival structure. High frequency oscillations were removed using a 10-day low pass filter. Results are shown in Figure 6 as a dot plot (the two large gaps in the dot plot correspond to outages addressed in Table 1). The dot plot allows identification of individual rays at the receiver location and match these to the modeled arrivals, which will be discussed in Chapter 3.

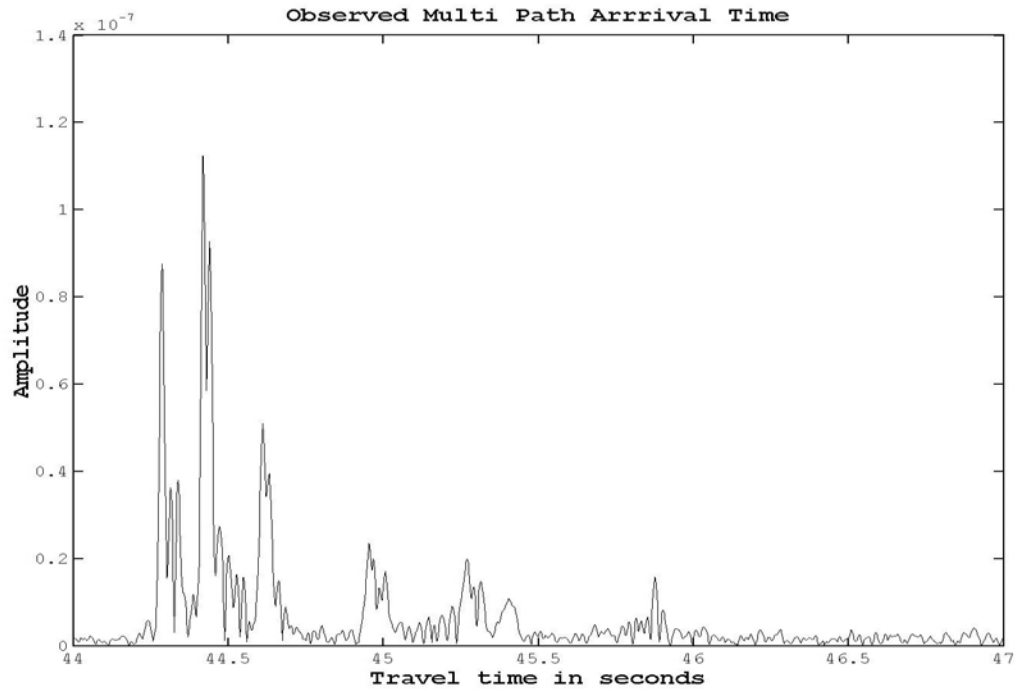


Figure 4 - Example of coherently averaged signal

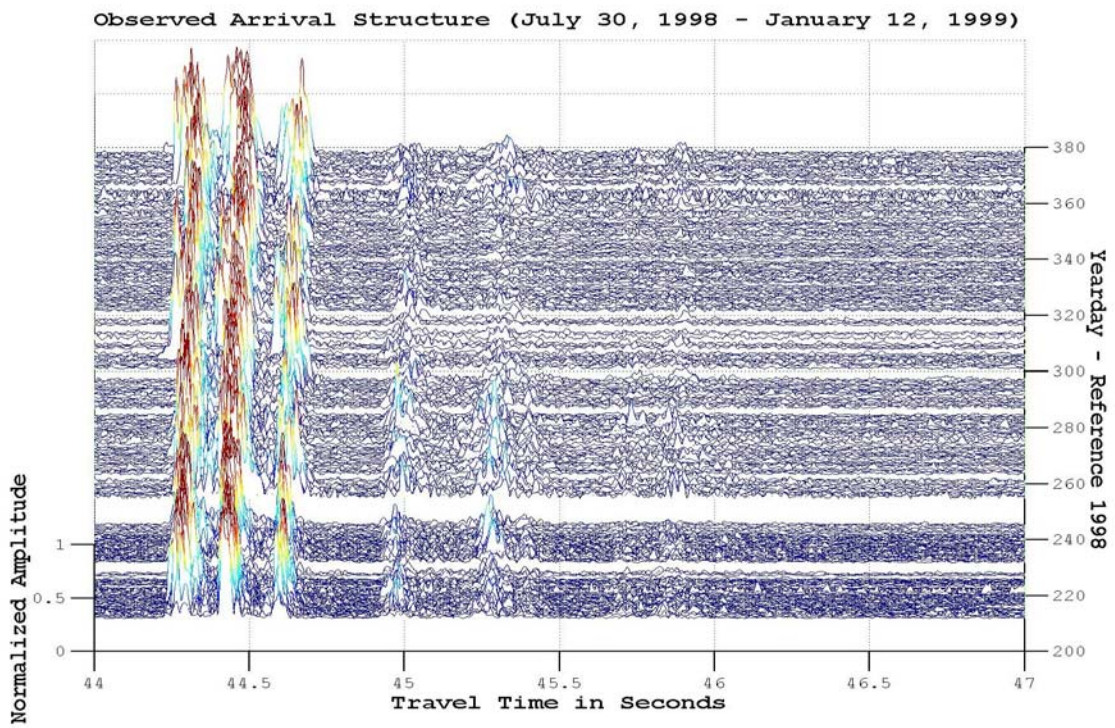


Figure 5 - Waterfall of observed arrival structure

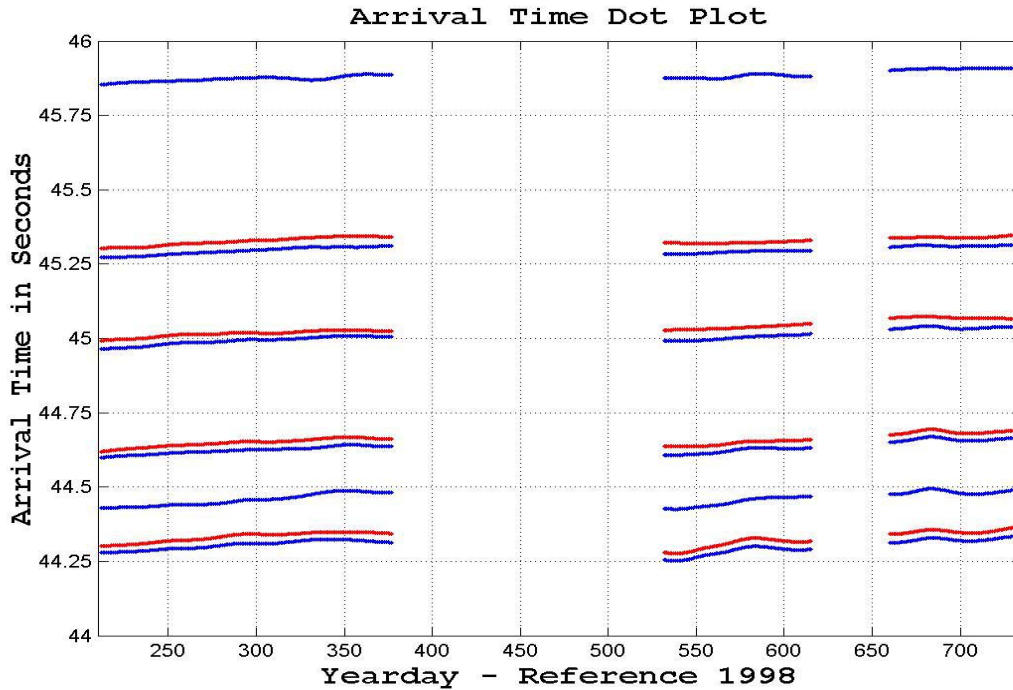


Figure 6 - Travel time dot plot of observed arrivals

## B. OCEANOGRAPHIC DATA

### 1. Shipboard Data

Acoustic modeling of the received signal requires creation of a "background" or "reference" ocean. One input required by the model is a reference sound speed profile. During July 1998, an oceanographic cruise aboard the R.V. POINT SUR provided CTD data at 9 stations along a path between Davidson Seamount and Sur Ridge. Based upon the CTD data, a mean sound speed profile was derived (Figure 7). This mean profile represents the reference ocean in forward modeling, and serves as an initialization for the inverse.

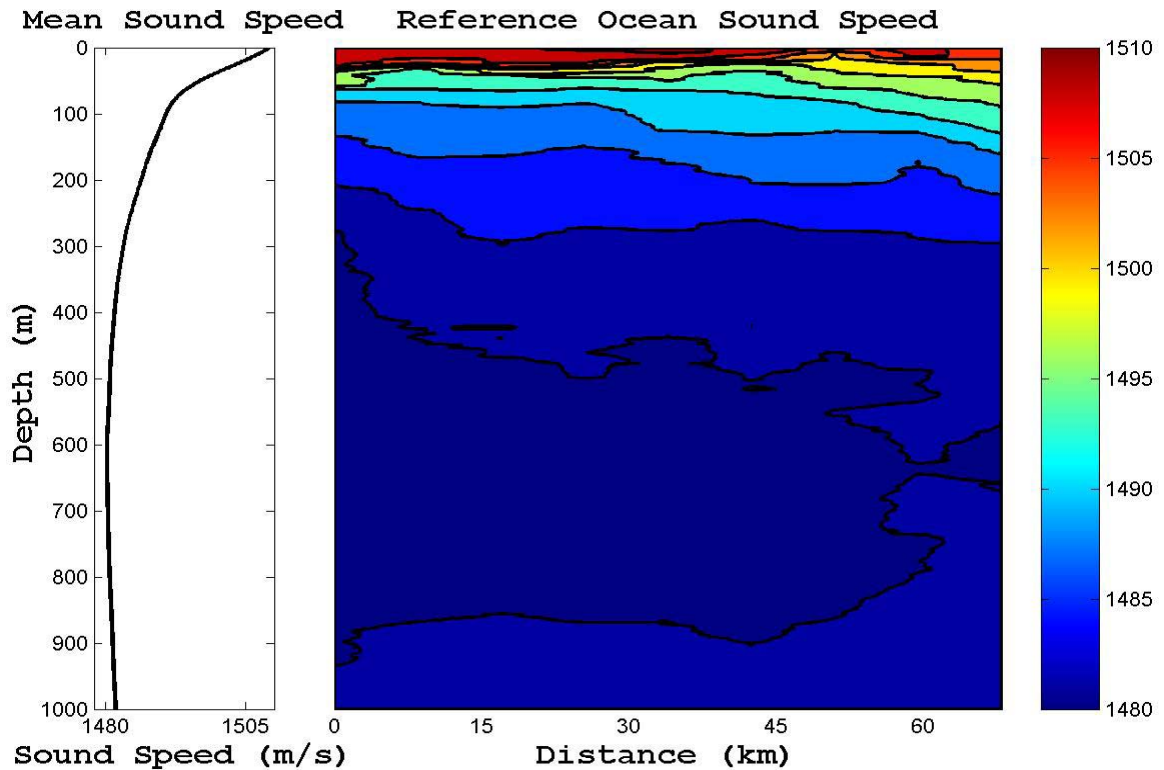


Figure 7 - Mean sound speed profile and reference sound speed field (upper 1000 m)

## 2. Moored Temperature Data

During the acoustic transmissions, oceanographic moorings M2 and M4, (deployed by MBARI and NPS, respectively) provided *in-situ* temperature data. The M2 time series covered the entire period of transmissions, recording temperature every 10 minutes at depths of 10, 20, 40, 60, 80, 100, 150, 200, 250 and 300 m. M4 included an additional temperature measurement at 350 m, but was only operational for the last four months of transmissions (September through December, 1999). Geographic locations of M2 and M4 are depicted in Figure 1. For an overall sense of ocean variability throughout the time series, M2 temperature variations are depicted in Figure 8.

M2 Temperature Data: August 1998 thru December 1999

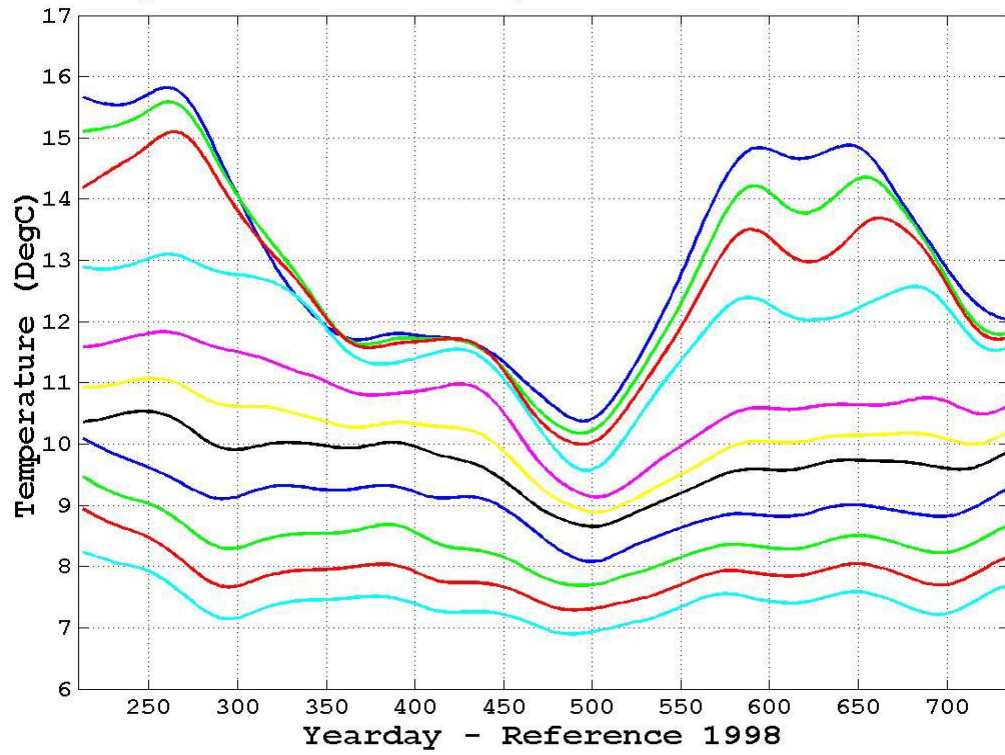


Figure 8 - Temperature variation at M2

THIS PAGE INTENTIONALLY LEFT BLANK

### III. FORWARD MODELING

#### A. HAMILTONIAN RAY TRACING

Ray theory allows the study of sound propagation through a medium whose refractive index can vary in space. Raytracing provides a graphical representation of the trajectories taken by sound energy through the medium. According to ray theory, the signal received is the sum of many different arrivals, each following different paths, or eigenrays, from the transmitter to receiver. Pressure disturbances at the receiver are associated with individual eigenrays, which have different phase shifts, time delays, and amplitudes. The received signal can be written as:

$$r(t) = \sum a_n s(t - t_n) e^{-i(2\pi f_0 t_n + \Phi_n)} \quad (1)$$

where  $r(t)$  is the complex envelope of the received signal,  $s(t)$  is the complex envelope of the emitted signal,  $f_0$  is the carrier frequency of the transmission, and  $t_n$ ,  $a_n$ , and  $\Phi_n$  are the time delay, amplitude modification and phase shift of each eigenray, respectively. Consequently, forward modeling of the received signal demands raytracing, eigenray search, and determination of  $t_n$ ,  $a_n$  and  $\Phi_n$ .

The three-dimensional raytracing program HARPO (Hamiltonian Acoustic Raytracing Program for the Ocean) was used to calculate raypaths. HARPO traces each raypath by numerically integrating Hamilton's equations of motion in spherical coordinates with a different set of initial conditions. In the high-frequency limit, sound waves behave like particles and travel along rays, according to the equations that govern changes of position and momentum

in a mechanical system (Jones *et al.*, 1986). HARPO requires input of a model ocean by the user, which consists of a continuous representation of the sound speed field and continuous two-dimensional representation of the upper and lower reflecting surfaces. The upper and lower reflecting surfaces are the ocean surface and ocean bottom, respectively. Continuous treatment of sound speeds and bathymetry eliminates the problems of false caustics and discontinuous raypath properties (Jones *et al.*, 1986). Since its inception, HARPO has undergone various modifications and improvements. Newhall *et al.* (1990) created supplementary peripheral routines for efficient eigenray finding and interpolation of gridded sound speed, current, and bathymetric data. Bathymetric and mean sound speed profiles used in HARPO for this study are shown in Figures 2 and 7, respectively.

Within HARPO, a fan of rays from  $-15^\circ$  to  $+15^\circ$  was traced at a resolution of  $0.002^\circ$ . Rays greater than  $15^\circ$  and less than  $-15^\circ$  were omitted due to numerous bottom interactions, which lead to a significant energy loss at the receiver.

## **B. ARRIVAL STRUCTURE**

The output of HARPO includes eigenray geometry and travel time. Processing of the HARPO output was accomplished using the program "ray2db" developed by Chiu (1994). This program searches for eigenrays, computes travel times, calculates phase shifts as a result of bottom and surface reflections, and estimates signal losses due to raytube spreading. Program "ray2db" operates on the HARPO

output file utilizing input parameters set by the user in the initialization program, "ray2dbstart". Input parameters include source and receiver separation, location and depth, source signal characteristics, and boundary condition parameters. Boundary conditions affect both the magnitude and phase of the eigenray arrivals through surface and bottom reflection. A root-mean-square sea surface height of 1 m represented the surface boundary condition. At the bottom boundary, complicated interactions of sound waves with the upper sea floor layer require geoacoustic modeling to compute general values and restrictive parameters for various marine sediment properties. These sediment properties vary between the source and receiver. At Davidson Seamount, the bottom is composed of rock outcroppings interspersed with coarse grained sediment, while at Sur Ridge the bottom is primarily coarser, glauconite-rich sediment (Gabriel, 2001). In between, the upper layer is generally comprised of fine to medium grain sediment. Based upon sediment chart and geoacoustic parameter tables (Hamilton, 1980), input parameters were determined for the bottom boundary (Table 4).

<b>Average sediment sound speed</b>	<b>1650 m/s</b>
<b>Average sediment density</b>	<b>1600 kg/m<sup>3</sup></b>
<b>Sediment attenuation rate</b>	<b>0.04 dB/m/kHz</b>

**Table 4 - Geoacoustic Parameters**

Given the HARPO output along with input parameters, "ray2db" computes the envelope of the received signal. The

modeled signal included 113 eigenrays, which are shown in Figure 9. The modeled arrival structure is shown in Figure 10 as a stem plot of the 113 individual arrivals.

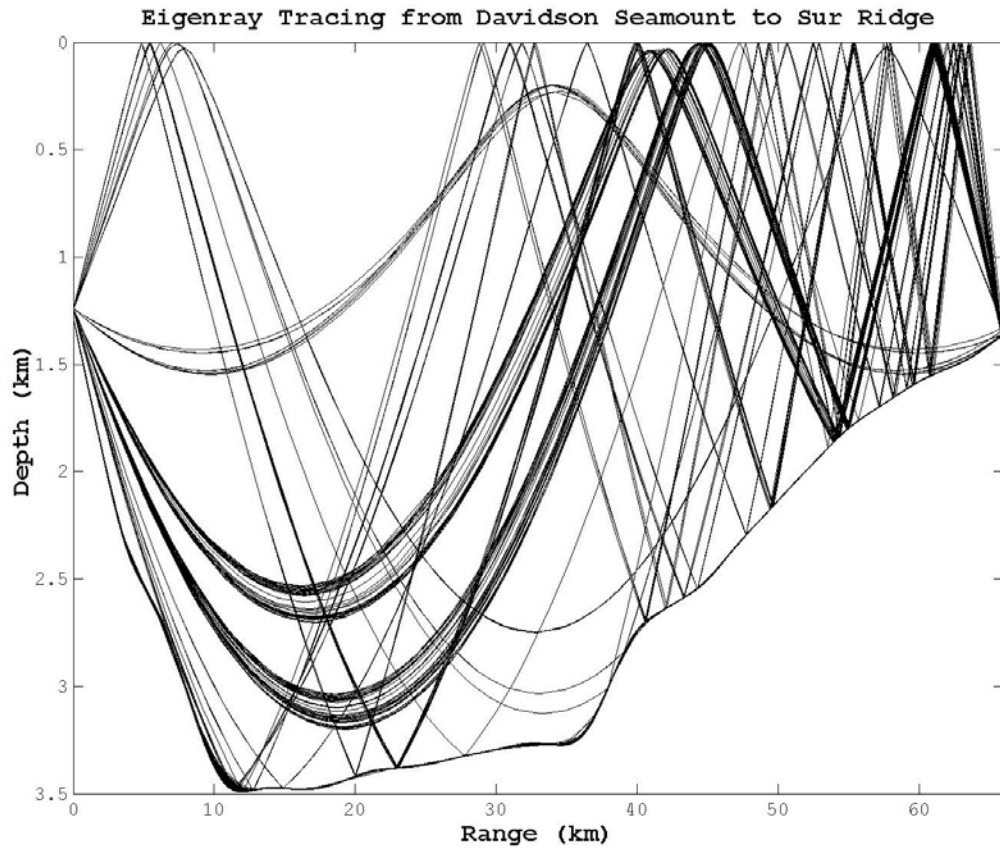
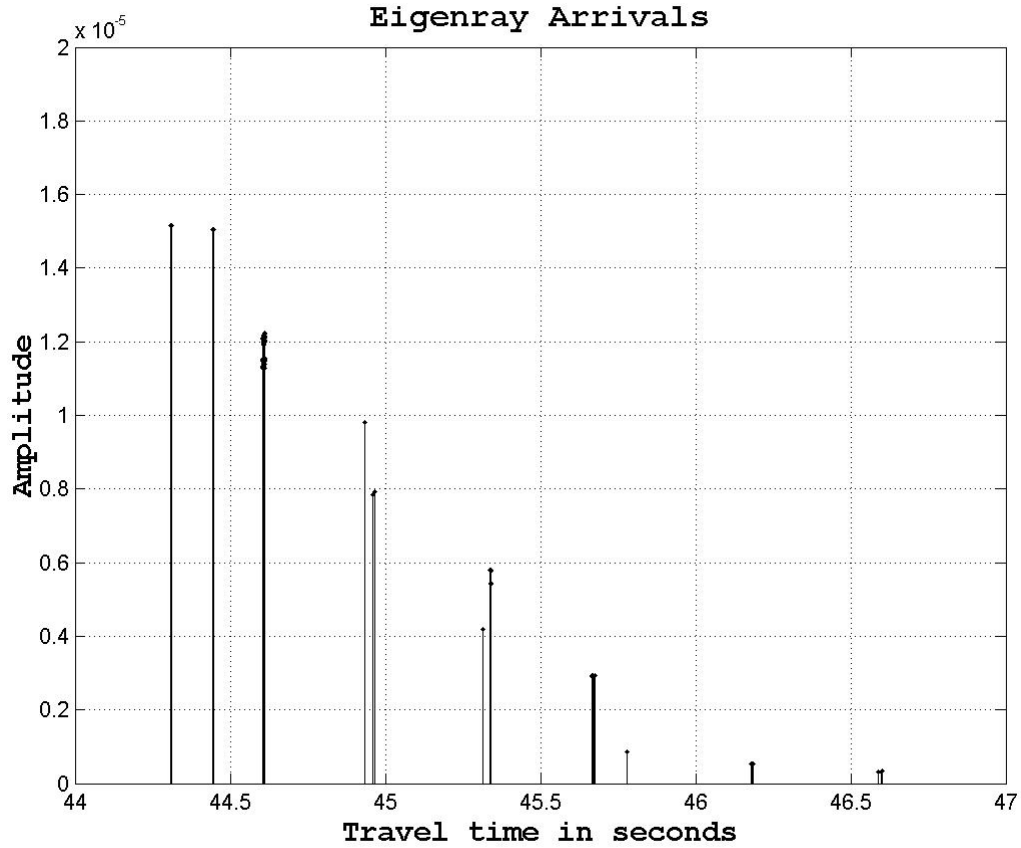


Figure 9 - Eigenray Geometry



**Figure 10 - Stem plot of individual eigenray arrivals**

The original modeled arrival time included a bias error associated with the actual source/receiver separation. An iterative least squares inversion was used to estimate the range error. A final range error estimation of 0.2496 km resulted in a travel time change of -166 ms. This estimated travel time change was then applied to the modeled rays, which assisted in identifying observed arrivals with model results.

### C. RAY IDENTIFICATION

Identification of ray arrivals was initially conducted by comparing the stem plot of the modeled eigenray arrivals (Figure 10) to the observed arrivals, waterfall plot and dot plot (Figures 4, 5 and 6, respectively). To further identify rays with observed arrivals, additional plots of the modeled arrivals were created. First, travel times versus launch angles were plotted, which revealed that each of the arrivals not only is associated with individual eigenrays but groups or "bands" of eigenrays with each band representing a set of micro-multipath that reach the receiver at the same time and sample the same space in the ocean. Next, a series of ray diagrams were constructed associating each eigenray band with each isolated arrival. Travel times versus launch angle are shown in Figure 11, while the geometry of the eigenray bands are shown in Figure 12.

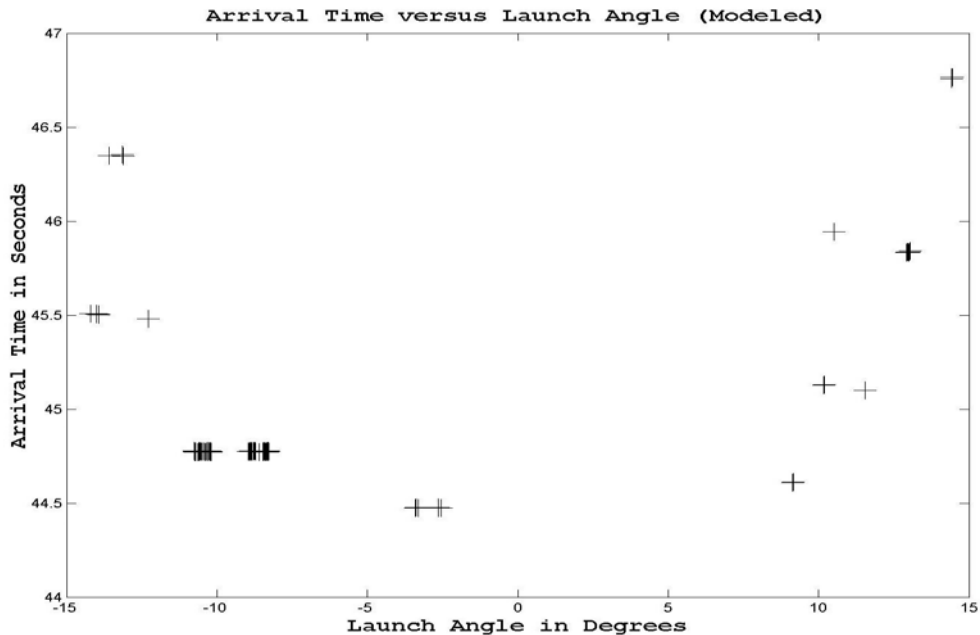


Figure 11 - Travel time versus launch angle (modeled)

### Arrival Bands 1-10

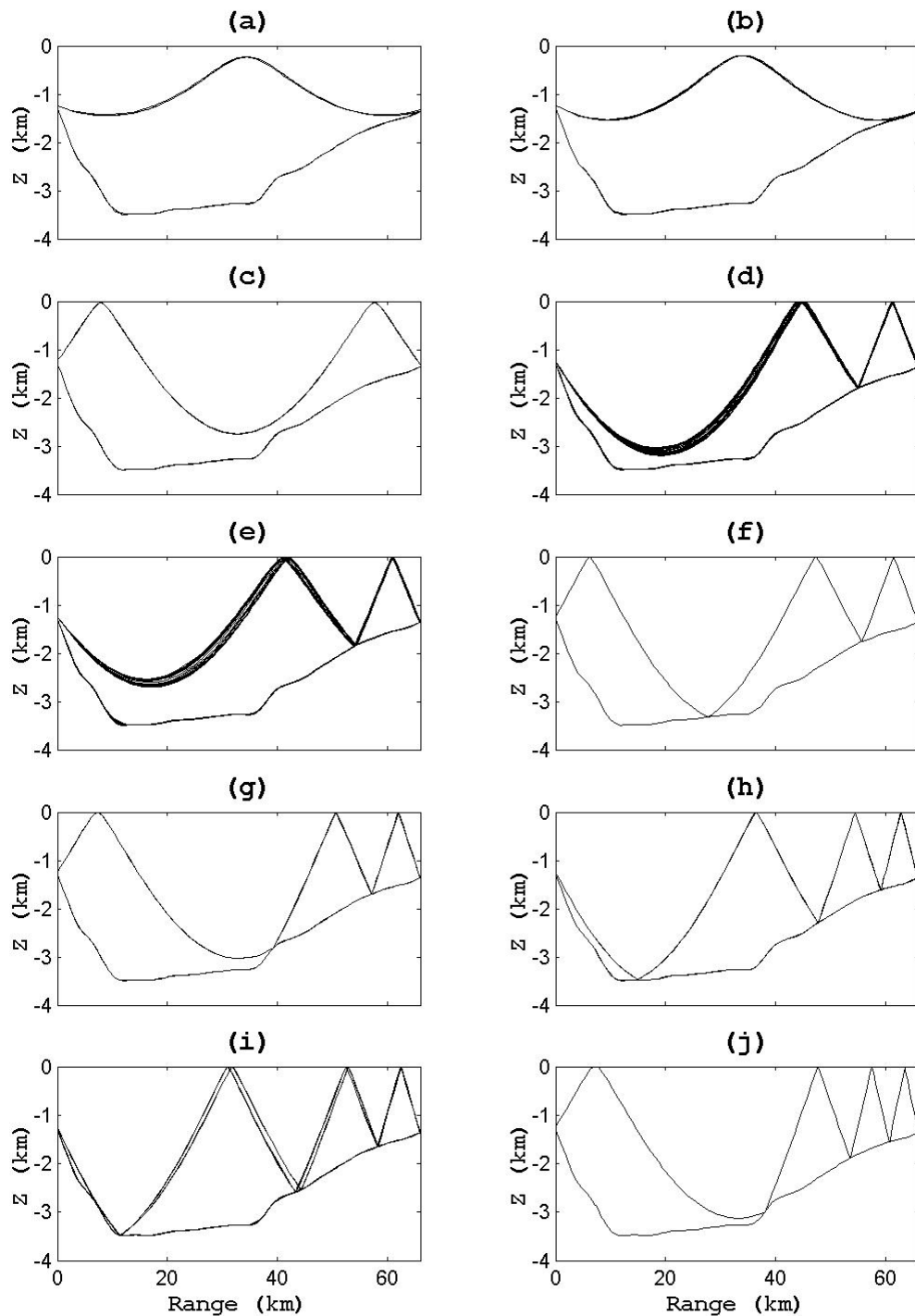


Figure 12 - Eigenray arrival bands

Using a combination of launch angle and arrival time a relationship was established between eigenray bands and observed arrivals. Each band of eigenrays was further examined to assist in identifying specific observed arrivals with modeled arrivals. Ten observed arrivals were associated with the 10-eigenray bands shown in Figure 12.

A band of nine eigenrays was identified in the modeled structure, but could not be identified as stable and resolvable arrivals in the observed data (e.g., a "ghost" arrival). Two additional bands of eigenrays were not identified in the observed data (Figure 13). Attenuation due to numerous surface and bottom bounces and deconstructive interference between the micro-multipaths may have contributed to a weak signal, unidentifiable in the presence of noise. These two unidentified rays are apparent in Figure 15, where their sound pressures are extremely low.

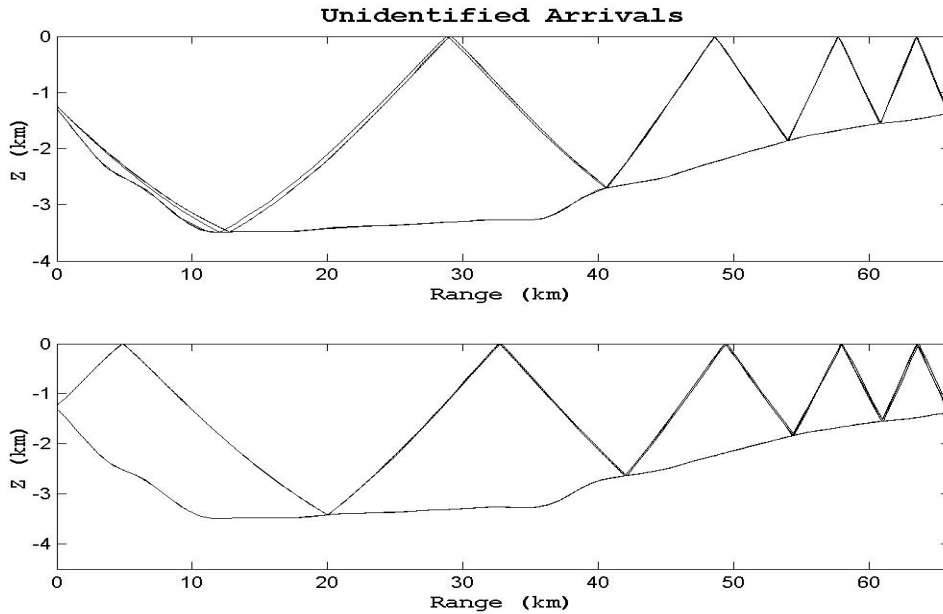


Figure 13 - Unidentified arrival bands

Once all modeled eigenrays bands were associated with particular observed arrivals (or were deemed unidentifiable), a single ray was chosen from each band to represent the path geometry of the band in the inversion. The eigenray geometry representing the 10 bands is depicted in Figure 14 while the modeled arrival structure is shown in Figure 15.

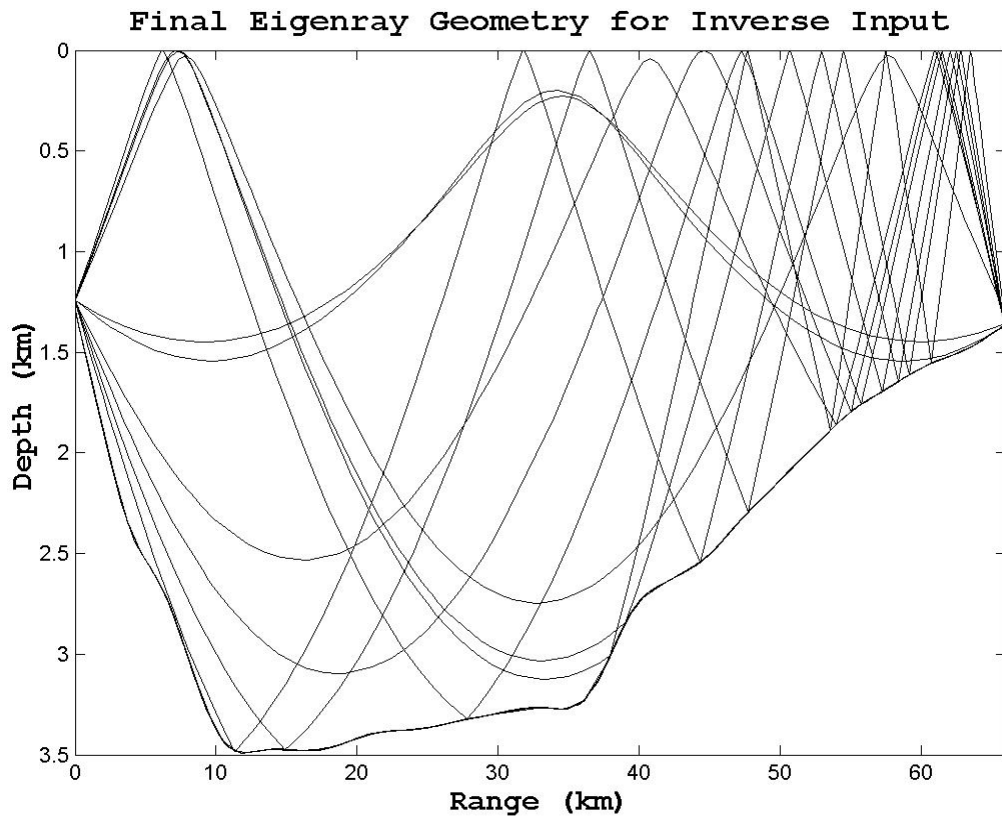


Figure 14 - Final 10 Eigenray Paths

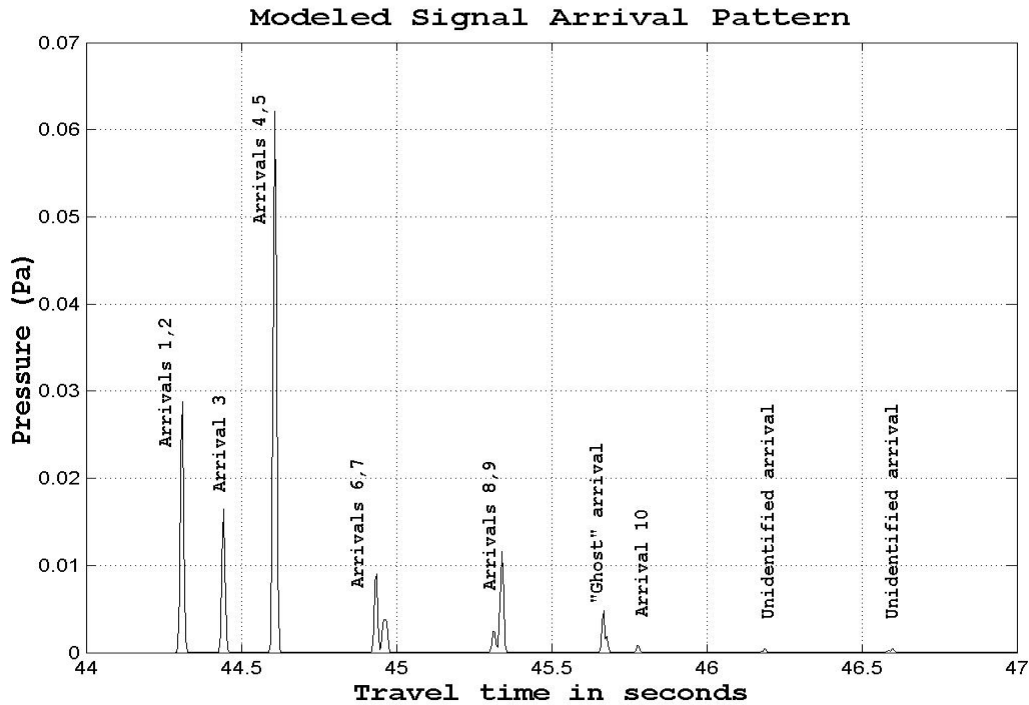


Figure 15 - Final modeled arrivals

**D. TRAVEL TIME VARIABILITY**

Sound speed in the ocean is a function of temperature, pressure and salinity, with temperature dominating in the upper 1000 m where the gradient is strongest. As the temperature increases, sound speed increases thus travel time decreases. Likewise, as the temperature decreases sound speed decreases and travel time increases. Known ocean processes can be directly related to temperature changes, which can then be observed as travel time changes. The principle objective of this experiment is to study the low frequency temperature variability between Davidson Seamount and Sur Ridge. Significant sources of low frequency oscillations in the ocean include seasonal or inter-annual change, synoptic scale events, and mesoscale

variations. Seasonal oscillations can be clearly seen in both the mooring and travel time data, which are characterized by cooling of the surface waters in winter and warming in summer. Synoptic scale events, such as upwelling and downwelling, are also evident in the mooring and travel time data. These types of events can be associated with northwest winds off Central California resulting in the upwelling of cool, nutrient rich waters, and south-southeast winds which result in a downwelling of warmer surface waters. Although present throughout the year, mesoscale variations may or may not be apparent in the mooring and travel time data simultaneously. These events can be much more localized, identified at one location (i.e., M4) and not the next (i.e., Davidson Seamount).

Semi-diurnal and diurnal variations, such as ocean tides and fluctuations in the mixed layer depth, were observed in the mooring and travel time data. These higher frequency oscillations were not the subject of this experiment and were filtered out using a 4<sup>th</sup> order, 10-day low pass filter.

THIS PAGE INTENTIONALLY LEFT BLANK

## IV. TOMOGRAPHIC INVERSE

### A. DEVELOPMENT OF THE INVERSE PROBLEM

Qualitatively, the inverse problem is relatively straightforward - infer the unknown ocean structure given the measurements of acoustic travel time along different raypaths. Quantitatively, the mathematical formulation requires some forethought. To apply inverse theory, a valid mathematical model must be established relating model parameters to measured data. A general mathematical expression used for ocean observing systems is the Fredholm integral equation of the first kind:

$$d(\underline{x}') = \int_I g(\underline{x}', \underline{x}) f(\underline{x}) d\underline{x} + e(\underline{x}') \quad (2)$$

where  $d(\underline{x}')$  is the data observed at some  $\underline{x}'$ ,  $g(\underline{x}', \underline{x})$  is the "model" or physics of the problem,  $f(\underline{x})$  is the unknown function, and  $e(\underline{x}')$  is the noise contamination. As opposed to a discrete observation, equation (2) represents a continuous observation over the space  $\underline{x}'$ , and linearly relates the data to the unknown. In this experiment the observed data is the perturbations of the travel times of the resolved rays, the model is the raypath output from HARPO, and the unknown is sound speed change.

Relating sound speed change to travel time change, the above equation can be expressed as:

$$\delta\tau_j = \int_{path_j} \left( \frac{-1}{c^2(\underline{x})} \right) \delta c(\underline{x}) ds + e(\underline{x}) \quad (3)$$

where  $\delta\tau_j$  is the change in travel time due to the sound speed perturbation  $\delta c$  along path  $j$ ,  $\bar{c}$  is the reference sound speed field,  $\delta c$  is the unknown variable which is the departure from the reference sound speed field,  $\underline{x}$  is the position vector and  $s$  is the arc length along the path  $j$  connecting the source and receiver. Contamination by noise is represented by  $e$ , and includes both measurement and model error.

The approach used will be a stochastic inverse method (Chiu *et. al*, 1994), which is based on a spectral decomposition of the sound speed perturbations and a minimization of an objective function. This method treats the unknowns as random variables, and requires specification of statistical information on the signal and noise. Specifying ocean decorrelation scales, a noise variance and a solution variance the method provides an optimal estimate of the solution, which has minimum mean square errors. To aid in oceanographic interpretation, the method also gives solution error and resolution estimates. Empirical Orthogonal Function Analysis (EOFA) on hydrographic data is employed to investigate the vertical structure for constraint in the tomographic estimate.

## **B. VERTICAL STRUCTURE AND CONSTRAINT**

EOFA is a common statistical method for analyzing oceanographic variability occurring across a spectrum of spatial and temporal scales. This method is used to redistribute the variability of a large set of variables to a much smaller set, which contains most of the original variance. In other words, EOFA estimates the spatial

variability and the time series coefficients modulating the temporal variability from the variance-covariance matrix of the observed data. The input is the observed data, while the output consists of three types of results, 1) principal components (PCs), 2) eigenvectors (EOFs), and 3) eigenvalues. The PCs, plotted as a time series, quantify the overall strength of the associated EOF pattern over time. The relative relationships between EOF points (or "modes") remain the same, but the absolute magnitude of the pattern changes with time.

An EOF analysis was constructed from the M2 mooring data. Modes 1-3 are shown in Figure 16. The analysis revealed that mode 1 was dominant, accounting for 54% of the variance. Modes 2 and 3 contained 22% and 8% of the variance, respectively. Simulation studies show that they do not contribute significantly to travel time change.

Additional deep CTD data analysis revealed the possibility of a phase change at 450-500 m and significant perturbations below 500 m. To account for the possible phase change and deep perturbations in the inverse, two additional layers were included. One can think of the intermediate (300-500 m) and deep (500-2000 m) layers as two additional EOFs with their unknown coefficients corresponding to layer-averaged perturbations. Figure 17 shows the 3-layer model that was used to constrain the vertical structure in the tomographic inverse.

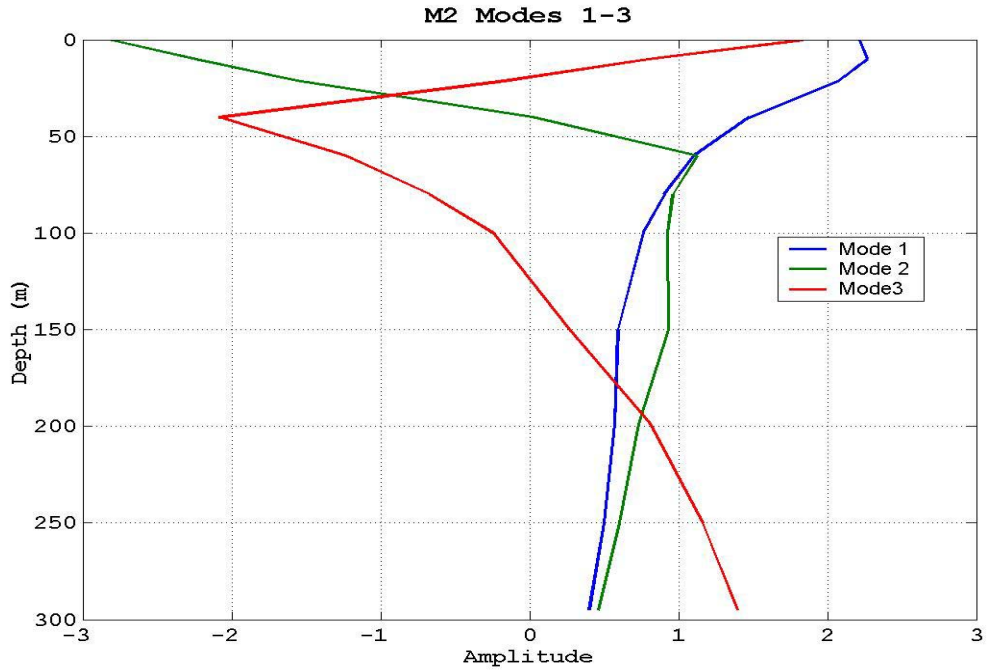


Figure 16 - M2 vertical structure

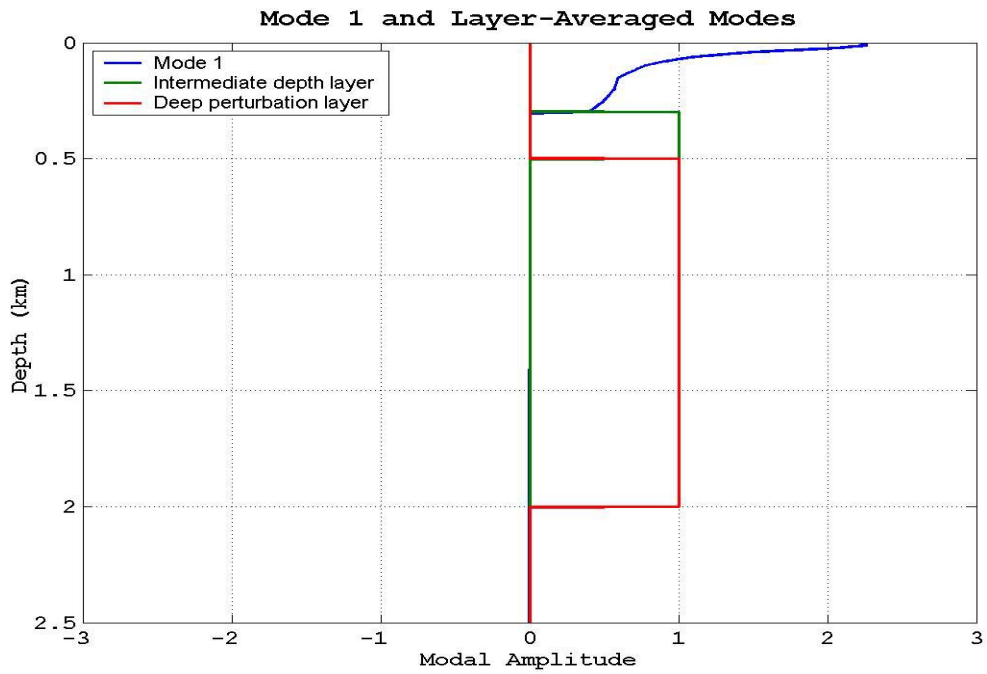


Figure 17 - Modes used for vertical constraint

### C. INVERSION

The change in sound speed is a function range, depth and time. This variation in sound speed can be described by a linear combination of  $n$  EOFs, i.e.,

$$\delta c(x, z, t) = \sum_{i=1}^n a_i(x, t) f_i(z) \quad (4)$$

where  $a(x, t)$  is the time and range varying amplitude of the EOF and  $f_i(z)$  is the  $i^{\text{th}}$  mode. In this description, the unknown becomes the coefficients of the EOFs. The horizontal variation of  $a_i(x, t)$  was discretized with a grid spacing of 1 km. The vertical structure was fixed with the first mode and two layer-averaged modes. The change in travel time is referenced to the first travel time measured, which coincides with the July 1998 CTD transect. An iterative solution was employed to refine the *a priori* statistical information, specifically the rms values of coefficients of perturbation EOFs and noise variance. The inverse method processes travel times for each iteration, giving daily estimates of sound speed perturbation. The solution was deemed valid when statistics of the final solution and data residual were consistent with the assumed values for the statistical parameters.

Several iterations of the inversion were used to refine the initial estimates. The input statistical parameters for the final iteration were  $64 \text{ (ms)}^2$  for the noise variance, 26 km for the horizontal decorrelation length,  $25 \text{ m}^2/\text{s}^2$  for the solution variance of mode 1,  $0.25 \text{ m}^2/\text{s}^2$  for the solution variance of the intermediate depth

layer, and  $1 \text{ m}^2/\text{s}^2$  for the solution variance of the deep perturbation layer.

#### **D. RESULTS AND DISCUSSION**

##### **1. Resolution and Mean Square Error of the Tomographic Estimate**

Horizontal resolution lengths of the tomographic estimate are depicted in Figure 18, and represent the smallest ocean feature that can be seen by tomography. Minimum resolution lengths of about 30-35 km occur for mode 1 and the deep perturbation at about 45 km in range, while for the intermediate mode the minimum resolution length of 39 km occurs at a range of 30 km. At ranges between 0 and 25 km, the density of raypath crossings is minimal, resulting in a poor resolution. Thus, in the first half of the transmission path, the tomographic system is unable to resolve ocean features that are shorter than the acoustic path. This poor resolution is also apparent near the receiver, where again the density of raypath crossings is minimal.

The mean square error (in percentage) or uncertainty in the estimate is shown in Figure 19. The estimated mode 1 coefficient has an average mean square error of less than 43%. For the intermediate depth layer the uncertainty in its coefficient estimate is 100%, which is due to the fact that the corresponding travel time signal is much less than the travel time noise. The deep perturbation layer has an average uncertainty of 50%.

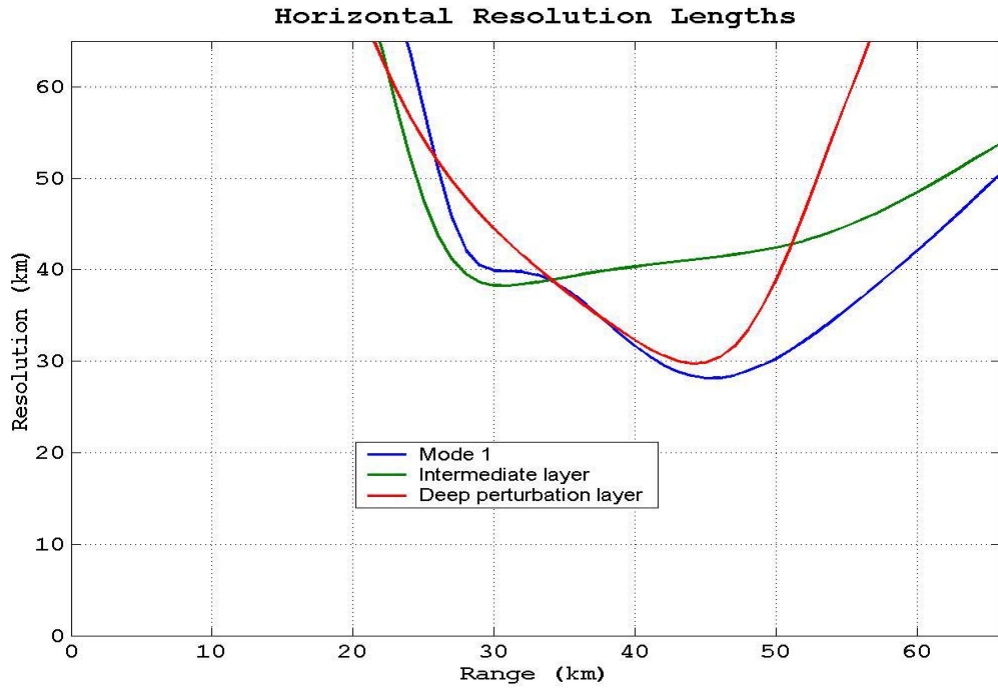


Figure 18 - Horizontal resolution lengths of the tomographic estimate

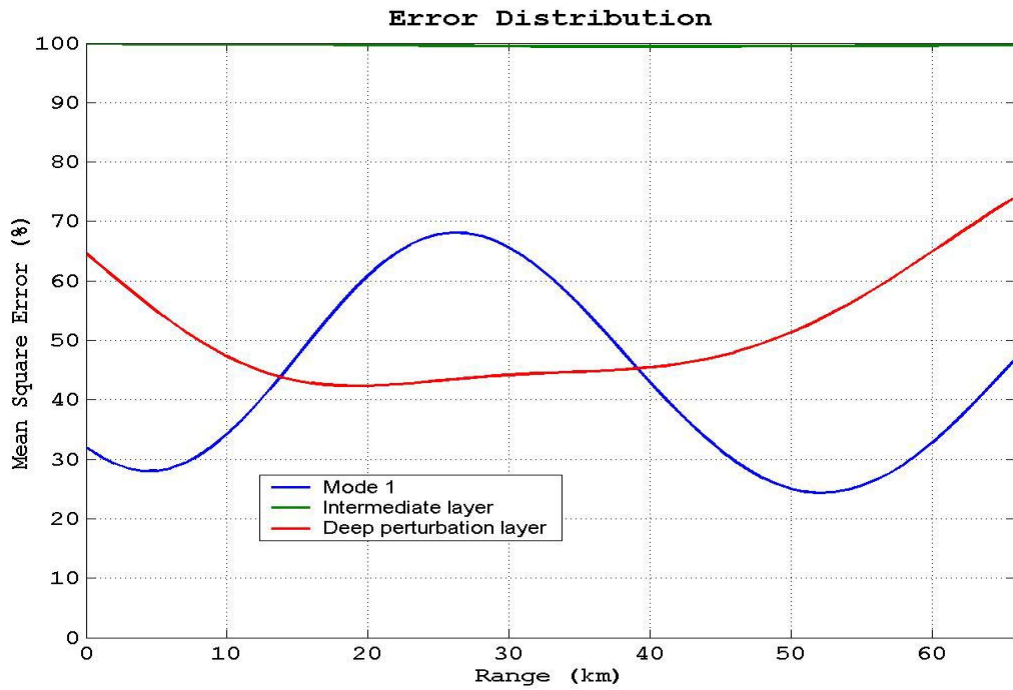


Figure 19 - Error distribution in physical space

## 2. Interpretation of Tomographic Estimate

Depth-averaged temperature perturbation estimates for mode 1 and the deep perturbation layer are shown in Figures 20 and 21, respectively. Both estimates show an initial zero perturbation at 1998 yearday 210, corresponding to initialization of the inverse to the first day travel time.

The mode 1 perturbation estimate was examined first. From 1998 yearday 210 to 375, the estimate showed a gradual cooling followed by a stronger cooling in the second half of the acoustic path. From 1998 yearday 575 to 735, the estimate showed cooling followed by slight warming, followed by stronger cooling. Once again the cooling is more defined in the second half of the acoustic path. This coincides with Figures 18 and 19, which show acceptable resolution and mean square error in this area. Although the error is acceptable in the first half of the acoustic path, the horizontal resolution indicates that the inverse was unable to adequately resolve ocean features smaller than the acoustic path.

The deep perturbation estimate showed gradual cooling followed by stronger cooling up to 1998 yearday 375. From 1998 yearday 535 to 735, the estimate revealed a strong warming followed by gradual and then deeper cooling. The error associated with the deep perturbation is marginal at best, with resolution lengths shorter than the acoustic path only between 20-55 km in range.

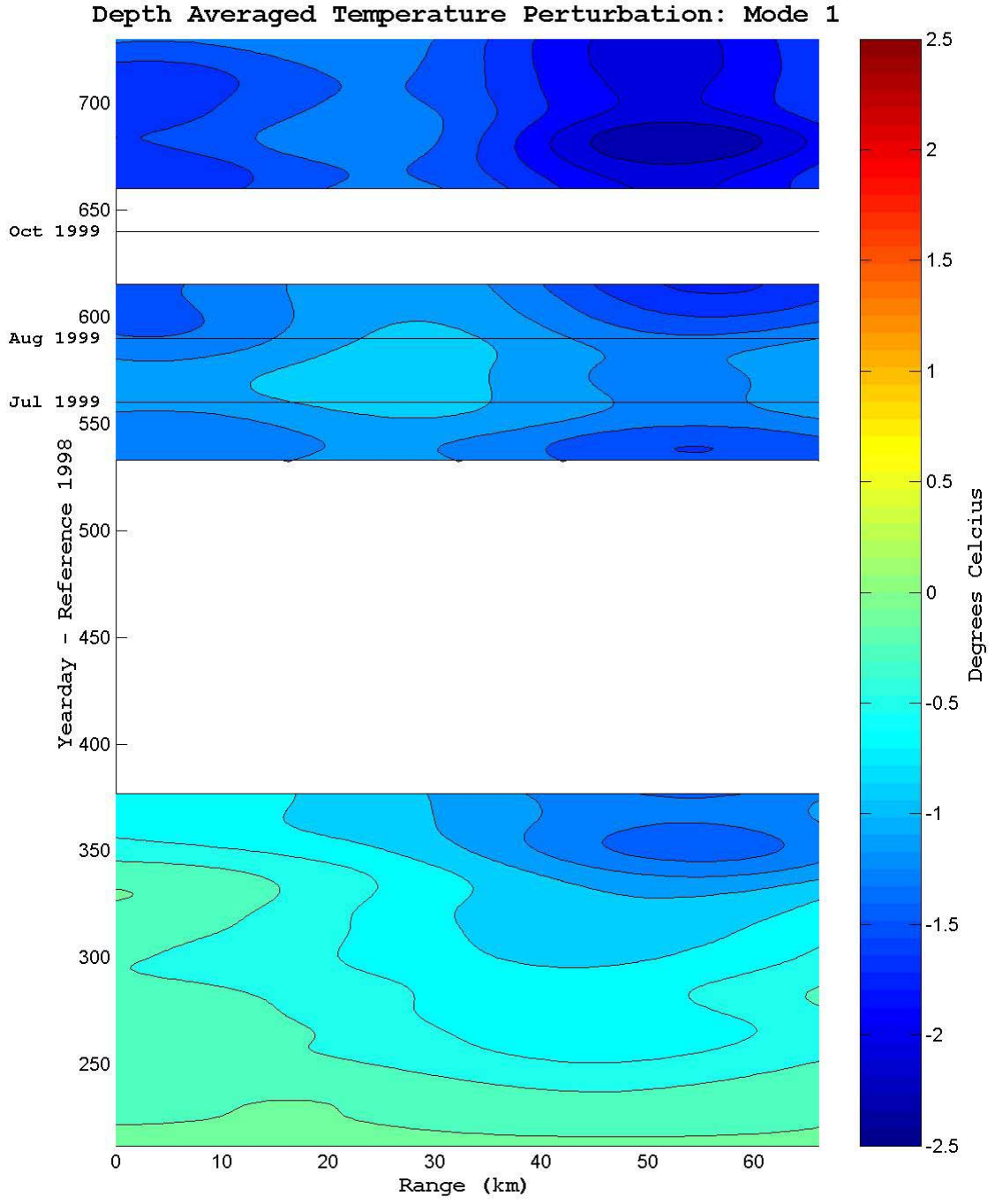


Figure 20 - Depth-averaged temperature perturbation estimate (mode 1, 0 - 300 m)

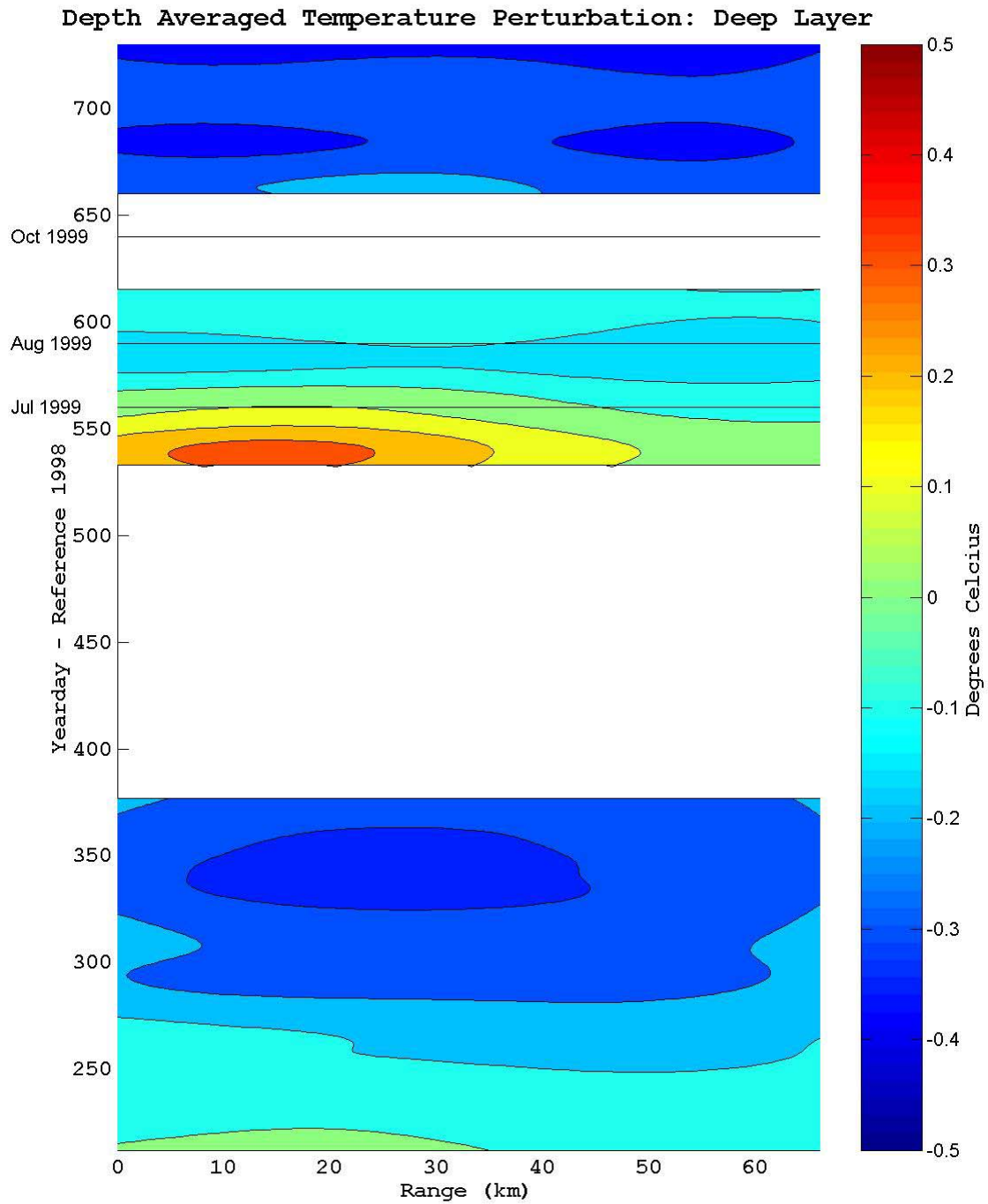


Figure 21 - Depth averaged temperature perturbation  
estimate (deep mode, 500 - 2000 m)

### 3. Comparison to Moored Temperature Data

Figure 22 shows M2 mode 1 coefficients along with range-averaged perturbation estimates for mode 1 and the deep perturbation layer (July 1998 - January 1999). The M2 perturbations signify a change from the M2 mean, while the range average perturbations signify a change from the first day. It is readily apparent that M2 mode 1 and the tomographic solution for mode 1 are in good agreement. Both show an overall cooling of similar magnitude in the upper layer where the mode reaches a maximum. The range-averaged solution for the deep perturbation shows a gradual cooling over the time series.

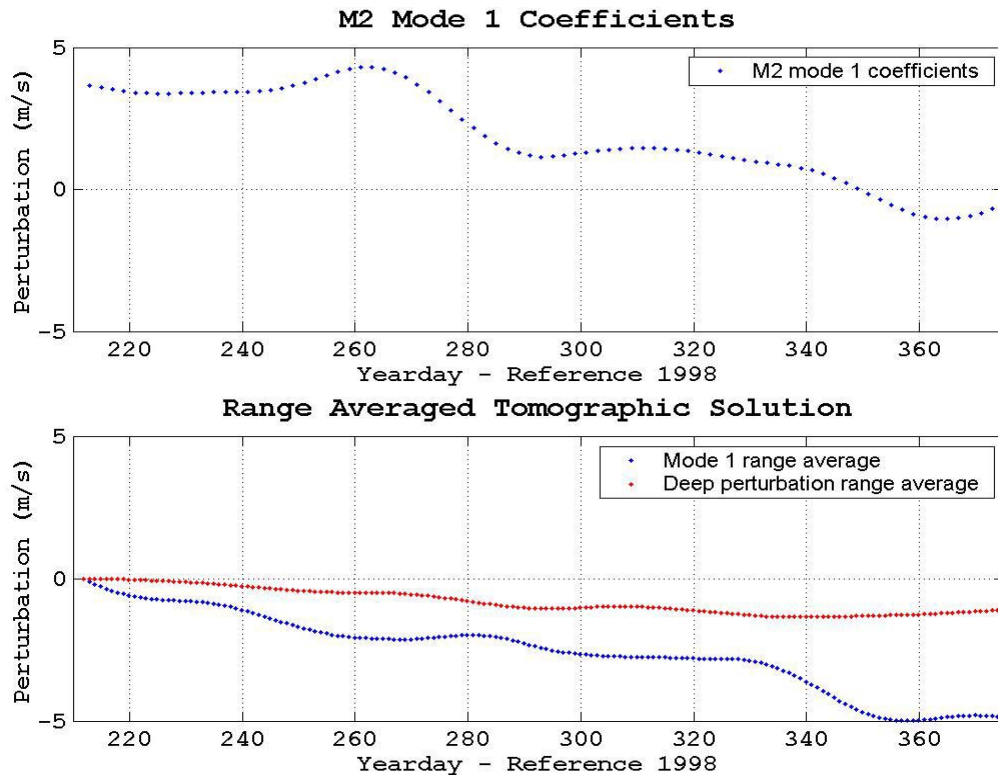


Figure 22 - Comparison of M2 mode 1 coefficients and range averaged tomographic estimate (July 1998 to January 1999)

Figure 23 shows M2 and M4 mode 1 coefficients along with range-averaged perturbation estimates for mode 1 and the deep perturbation layer (June 1999 - December 1999). The M2 and M4 perturbations signify a change from the M2 mean, while the range average perturbations signify a change from the first day. The overall warming and cooling trends of the mode 1 tomographic estimate are in general agreement with the mooring coefficients, except that the magnitude of the tomographic estimate is much larger than the M2 and M4 coefficients. This may be due to a localized cooling event along the acoustic path. The deep perturbation estimate shows slight warming followed by gradual cooling over the time series.

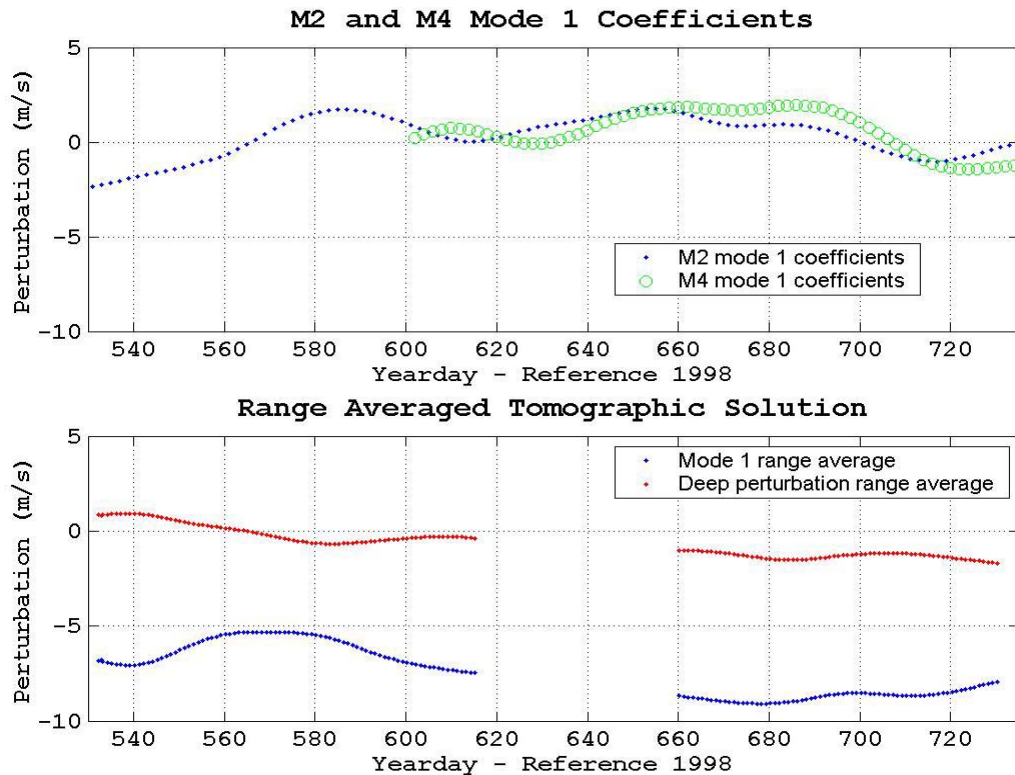


Figure 23 - Comparison of M2 and M4 coefficients, and range averaged tomographic estimate (June 1999 to December 1999)

#### 4. Comparison to CTD Transects

As a consistency check on the tomographic estimate, temperature data from CTD transects along the acoustic path were examined. For comparison purposes, the July 1998 reference section is shown alongside the July 1999, August 1999 and October 1999 sections (Figures 24, 25 and 26, respectively). To assist in examining the deep perturbation layer, deep mooring data from a current meter at M2 and a CTD at the source are shown in Figure 27.

The mode 1 perturbation estimate (Figure 20) was examined first. Comparing the July 1998 (1998 yearday 195) and July 1999 (1998 yearday 560) temperature sections (Figure 24), significant cooling was visible throughout the upper 300 m. Overall, this compares well with the perturbation estimate. Localized events along the acoustic path were further examined, specifically along the second half of the acoustic path. During July 1999 (1998 yearday 560), the perturbation estimate showed regions of warmer water surrounded by cooler water, corresponding to positive and negative perturbations, respectively. Upon inspection of the July 1999 (1998 yearday 560) temperature section, significant warming was evident, particularly at depths of 200-300 m near the receiver. This warming signature may be due to an increase in strength of the California Undercurrent as the "spring transition" relaxes. The August 1999 (1998 yearday 590) temperature section (Figure 25) showed a reversal of the isotherms near the receiver. This cooling signature can be seen as "more negative" perturbations in the tomographic estimate, which may be indicative of a relaxation of the California Undercurrent.

The October temperature section (Figure 26) showed further overall cooling across the 0-300 m layer, which corresponds to the stronger negative perturbations across the gap (October 1999 (1998 yearday 640) falls within the data gap).

The depth-averaged perturbation estimate for the deep layer was examined next. Comparing the July 1998 and July 1999 temperature sections (Figure 24) between 500 and 1000 m, a slight warming or pushing down of the isotherms was visible in the first 30 km. This was apparent in the perturbation estimate, which showed warming over the depth averaged layer. Analysis of deep temperature data at the source (Figure 27) was consistent with initial seasonal cooling followed by overall warming. The August 1999 (1998 yearday 590) temperature section (Figure 25) showed additional warming in the deeper layers while the estimate revealed a gradual cooling over the depth-averaged layer. The October 1999 section (Figure 26) showed a reversal of the isotherms. A data gap in the estimate precludes comparison with tomography, however, this cooling was apparent later in the estimate and was consistent with the seasonal cooling visible in the deep mooring data. In the second half of the acoustic path, the July 1999 (1998 yearday 560) temperature section revealed a dominant cooling event followed by slight warming near the receiver, while the August 1999 (1998 yearday 590) section revealed warming followed by slight cooling. The overall cooling signature was apparent in the perturbation estimate, however, the slight warming signature at the receiver was not. The October 1999 (1998 yearday 640) temperature section showed significant cooling along the second half of

the acoustic path, which can be interpolated in the estimate across the data gap. In addition, the seasonal cooling was readily apparent in the deep mooring data.

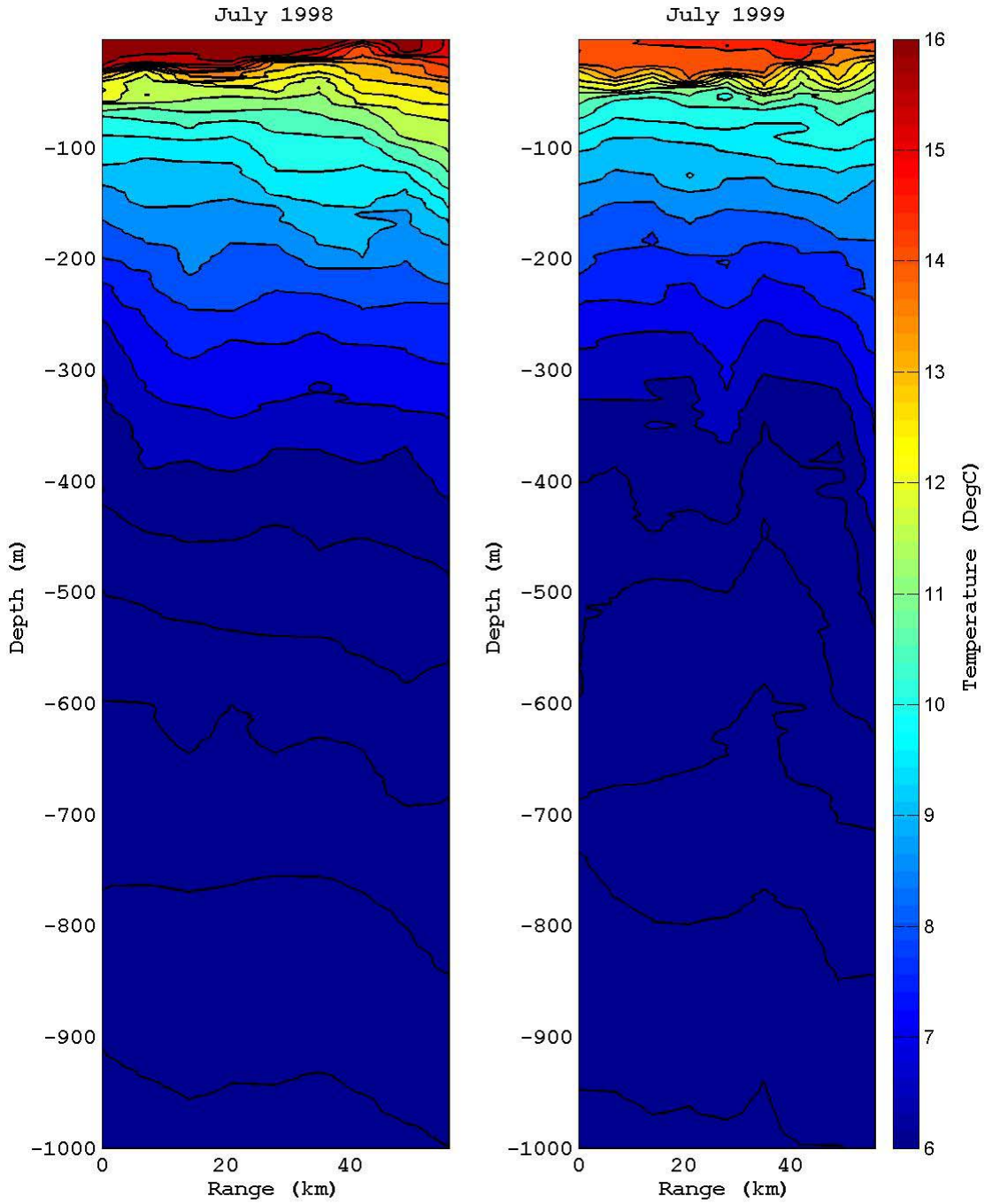


Figure 24 - Temperature data from July 1998 and July 1999  
transect along acoustic path

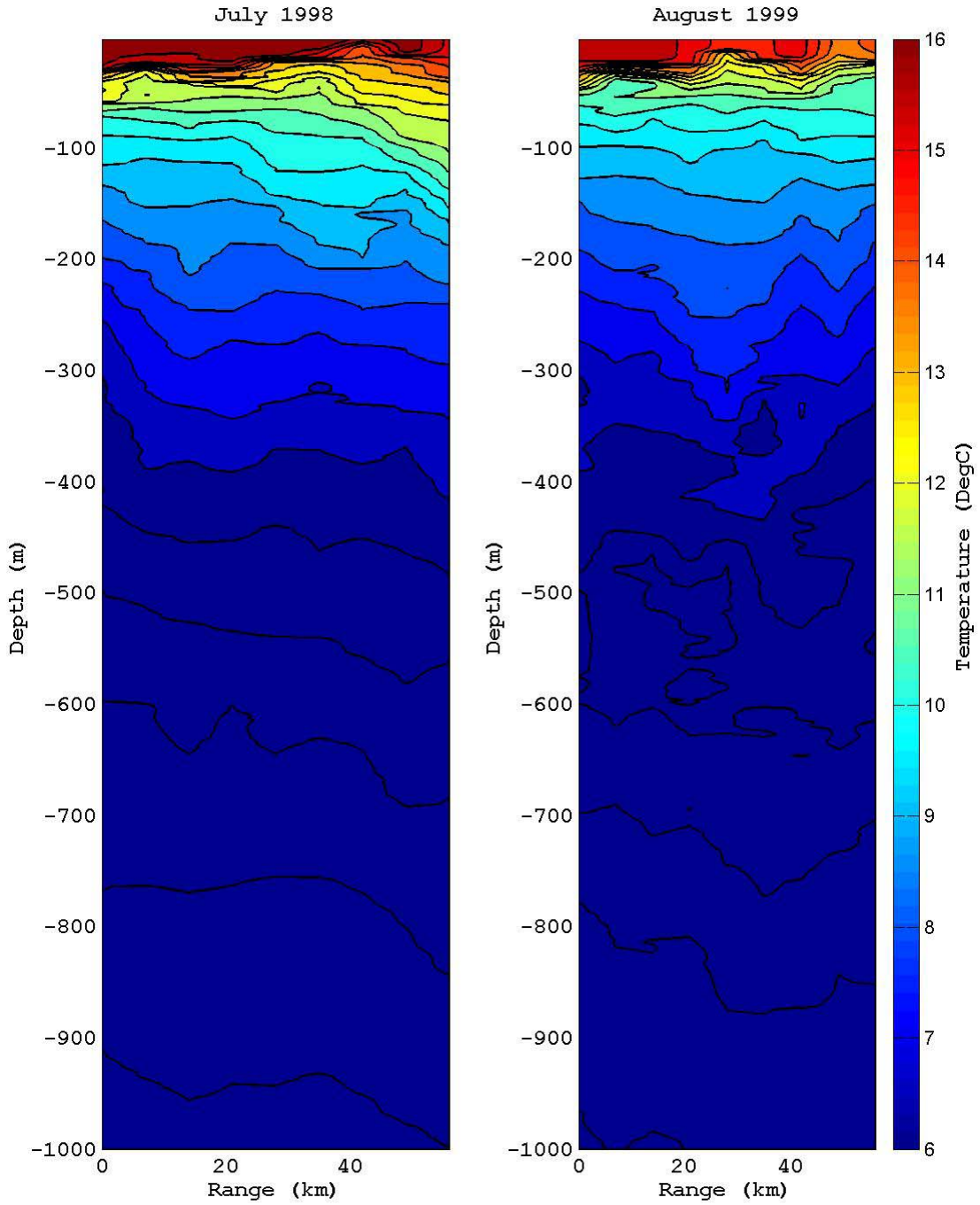


Figure 25 - Temperature data from July 1998 and August 1999 transect along acoustic path

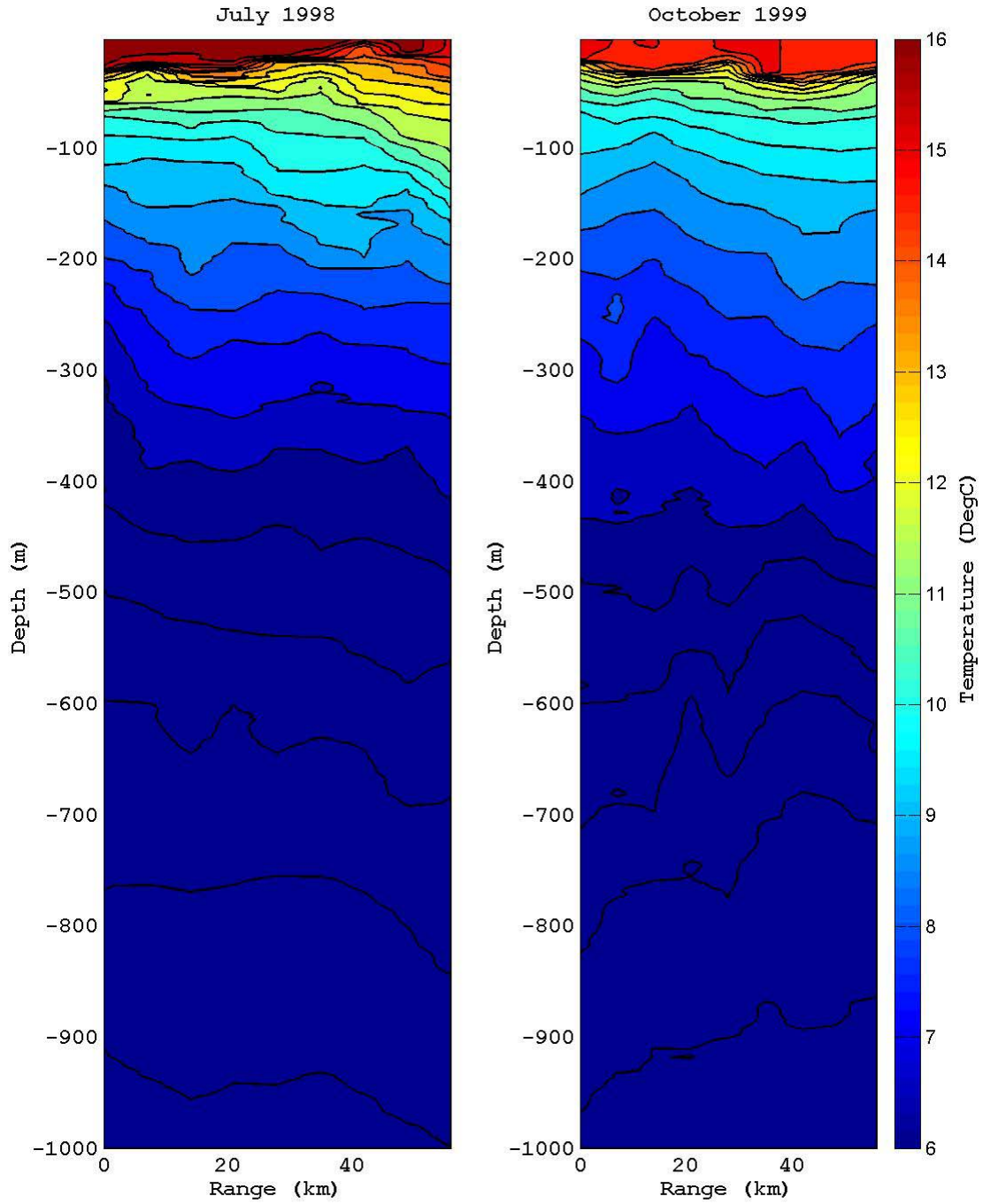


Figure 26 - Temperature data from July 1998 and October 1999 transect along acoustic path

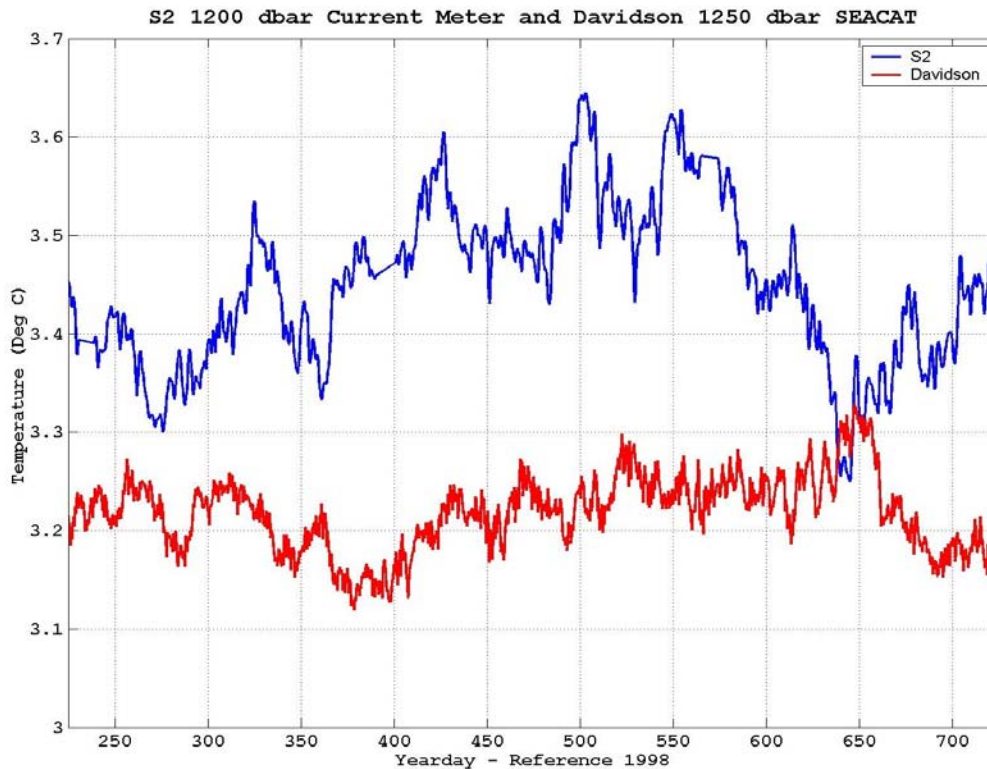
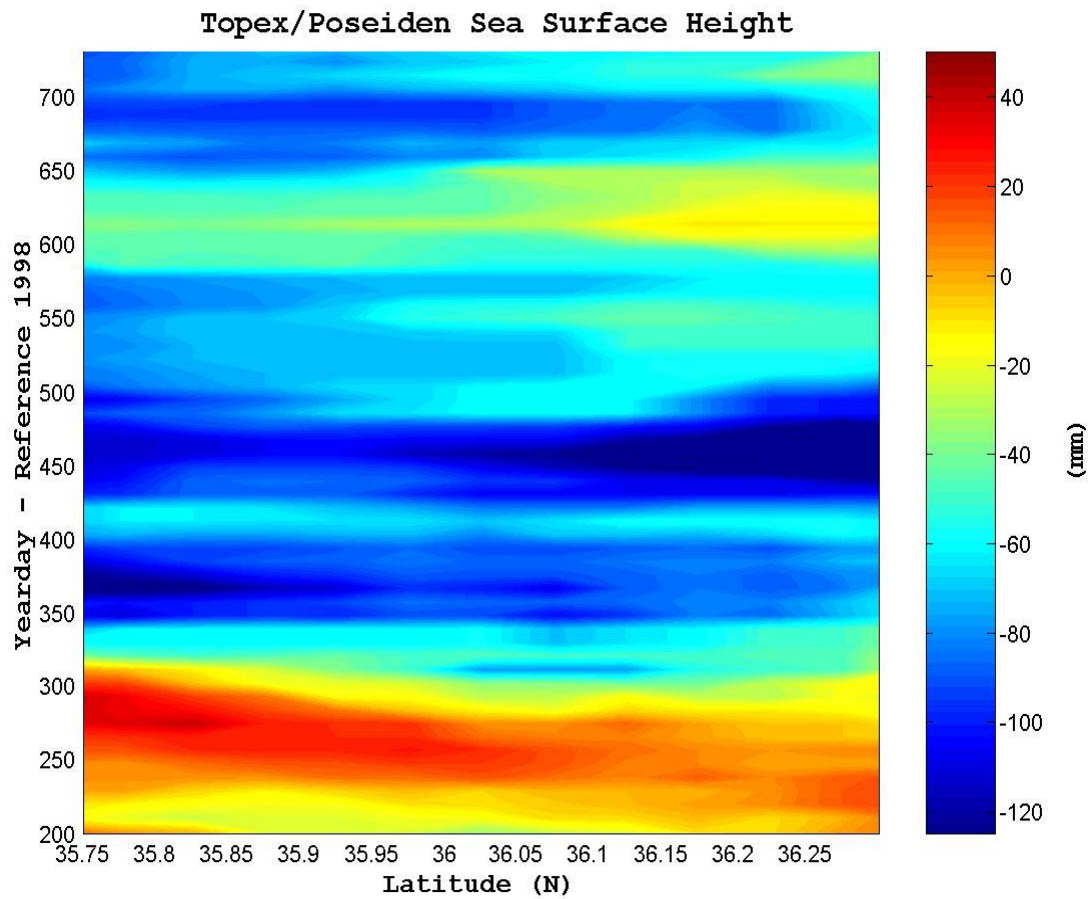


Figure 27 - Deep mooring temperature data at source and M2

### 5. Comparison to TOPEX/POSEIDEN Altimetry

TOPEX/POSEIDEN sea surface height anomalies in the vicinity of the acoustic path were examined over the tomographic time series. The altimetry data (Figure 28) is in general agreement with the mode 1 perturbation estimate (Figure 20). Tomography shows a warm ocean followed by strong cooling, consistent with the change in sea surface height. An exception is near the source, where the altimetry shows stronger cooling. From 1998 yearday 550 and later, tomography shows a cooler ocean. A noticeable correlation was observed in the vicinity of 1998 yearday 675, where the estimate shows a strong cooling, which is consistent with the lower sea surface height shown in the

altimetry data. The high sea surface height visible in the altimetry in the vicinity of 1998 yearday 600-650 is not apparent in the tomographic data. This is most likely due to late summer surface warming, which was not detected by the depth-averaged tomography.



**Figure 28 - TOPEX/POSEIDEN sea surface height**

## V. CONCLUSIONS

The objectives of this thesis were to examine temperature variability between Davidson Seamount and Sur Ridge using ocean acoustic tomography. The study included solving the forward problem, identifying modeled rays with observed arrivals, and inverting travel time perturbations using a stochastic inverse method. In solving the forward problem, a ray-theory approach was used to model the arrival pattern. Modeled rays were associated with 10 observed arrival peaks, and the time series of observed travel times were extracted. The vertical structure was constrained using a 3-layer model consisting of a dominant surface intensified mode, an intermediate depth layer and a deep perturbation layer. An iterative solution was used to refine the estimated statistical parameters, to arrive at a best estimate of the temperature perturbation field. Based on the estimated perturbations, coastal ocean variability along the transmission path was examined.

The following summarizes major findings of this thesis:

- 1) Horizontal resolution was poor near the source and receiver. Since eigenray geometry determines the horizontal and vertical resolving power, a lack of raypath crossings results in poor resolution. Higher resolution could be obtained by locating the source and receiver closer to the sound channel axis.
- 2) The vertical structure was not well represented by 1 mode. A 3-layer model was used to constrain the

vertical in the tomographic estimate. An EOF analysis on M2 hydrographic data resulted in a surface dominated mode, which represented the upper 300 m. Additional deep CTD analysis revealed a possible phase change at 450-500 m and perturbations below 500 m. To account for possible phase changes and deep perturbations in the inverse, two additional layers (300-500 m and 500-2000 m) were included as two EOFs with their unknown coefficients corresponding to layer-averaged perturbations.

- 3) The tomographic estimate was compared to *in situ* mooring data, CTD transects along the acoustic path, and TOPEX/POSEIDEN satellite altimetry. Comparisons show that the tomographic estimate has high enough spatial and temporal resolution to distinguish seasonal and mesoscale oscillations. The time series was dominated by significant cooling and warming events, which may have masked additional mesoscale fluctuations.

## LIST OF REFERENCES

- Birdsall, T.G., and K. Metzget, "Factor Inverse Matched Filtering," *J. Acoustic Society of America*, 79(1), 91-99, 1986.
- Chiu, C.-S., J.F. Lynch, and O.M. Johannessen, "Tomographic Resolution of Mesoscale Eddies in the Marginal Ice Zone: A Preliminary Study," *J. Geophys. Res.*, Vol. 92, NO. C7, 6886-6902, 1987.
- Chiu, C.-S., A.J. Semtner, C.M. Ort, J.H. Miller, and L.L. Ehret, "A Ray Variability Analysis of Sound Transmissions from Heard Island to California," *J. Acoustic Society of America*, Vol. 96(4), 2380-2388, 1994.
- Chiu, C.-S., J.H. Miller and J.F. Lynch, "Inverse Techniques for Coastal Acoustic Tomography," in *Environmental Acoustics*, D. Lee and M. Schultz, Eds., *World Scientific*, 1994a.
- Collins, C.A., R.G. Paquette, and S.R. Ramp, "Annual Variability of Ocean Currents at 350-M Depth over the Continental Slope off Point Sur, California," *CALCOFI Rep.*, Vol. 37, 257-263, 1996.
- Gabriel, C.L., "The Physical Characteristics of Bottom Sediment Near Sur Ridge, California," Master's Thesis, Naval Postgraduate School - Monterey, CA, March 2001.
- Hamilton, E.L., "Geoacoustic Modeling of the Sea Floor," *J. Acoust. Soc. Am.*, 68(5), 1313-1338, 1980.
- Hickey, B.M., "The California Current System: Hypothesis and Facts," *Prog. Oceanogr.*, 8, 191-279, 1979.
- Hickey, B.M., "Coastal Oceanography of Western North America From the Tip of Baja California to Vancouver Island," *The Sea, Volume 11*, 345-393, 1998.
- Huyer, A., and R.L. Smith, "A Subsurface Ribbon of Cool Water Over the Continental Shelf off Oregon," *J. Phys. Oceanogr.*, 4, 381-391, 1974.

Jones, R.M., J.P. Riley, and T.M. Georges, "HARPO: A Versatile Three-Dimensional Hamiltonian Ray Tracing Program for Acoustic Waves in Ocean with Irregular Bottom", Wave Propagation Laboratory, National Oceanic and Atmospheric Administration, Boulder, CO, 1986.

Lynn, R.J., and J.J. Simpson, "The California Current System: The Seasonal Variability of its Physical Characteristics," *J. Geophys. Res.*, 92, 12,947-12,966, 1987.

Medwin, H., C.S. Clay, *Fundamentals of Acoustical Oceanography*. Academic Press. San Diego, CA, 1998.

Miller, C., "Estimating the Acoustic Modal Arrivals Using Signals Transmitted from Two Sound Sources to a Vertical Line Hydrophone Array in the 1996 Shelfbreak Primer Experiment," Master's Thesis, Naval Postgraduate School - Monterey, CA, June 1998.

Munk, W and C. Wunsch, "Ocean Acoustic Tomography: A Scheme for Large Scale Monitoring," *Deep Sea Research*, Vol. 26A, 123-161, 1979.

Newhall, A.E., J.F. Lynch, C.-S. Chiu, and J.R. Daugherty, "Improvements in Three-dimensional Hamiltonian Ray Tracing Codes for Underwater Acoustics," in *Computational Acoustics: Ocean Acoustic Models and Supercomputing*, edited by D. Lee, A. Cakmak, and R. Vichnevetsky, North-Holland, Amsterdam, 1990.

Paduan, J.D, L.K. Rosenfeld, S.R. Ramp, F. Chavez, C.S. Chiu, and C.A. Collins, "Development and Maintenance of the ICON Observing System in Monterey Bay." *Proceedings, American Meteorological Society's Third Conference on Coastal Atmospheric and Oceanic Prediction and Processes*, New Orleans, LA, 3-5 November, 226-231, 1999.

Pavlova, Y.V., "Seasonal Variations of the California Current," *Oceanology*, 6, 806-814, 1966

Reid, J.L., and R.A. Schwartzlose, "Direct Measurements of the Davidson Current off Central California," *J. Geophys. Res.*, 67, 2491-2497, 1962.

Spindel, R.C., and P.F. Worcester, "Technology in Ocean Acoustic Tomography," *J. Marine Tech. Soc.*, 20(4), 68-72, 1986.

THIS PAGE INTENTIONALLY LEFT BLANK

## INITIAL DISTRIBUTION LIST

1. Defense Technical Information Center  
Ft. Belvoir, VA
2. Dudley Know Library  
Naval Postgraduate School  
Monterey, CA
3. Moss Landing Marine Laboratory Library  
Moss landing, CA
4. Matthew Fontaine Maury Oceanographic Library  
Naval Oceanographic Office  
Stennis Space Center, MS
5. Dr. Mary L. Batteen  
Oceanography Department, Naval Postgraduate School  
Monterey, CA
6. Dr. Ching-Sang Chiu  
Oceanography Department, Naval Postgraduate School  
Monterey, CA
7. Dr. Curtis Collins  
Oceanography Department, Naval Postgraduate School  
Monterey, CA
8. Dr. Steve Ramp  
Oceanography Department, Naval Postgraduate School  
Monterey, CA
9. Dr. Jeffery Paduan  
Oceanography Department, Naval Postgraduate School  
Monterey, CA
10. Dr. Leslie Rosenfeld  
Oceanography Department, Naval Postgraduate School  
Monterey, CA
11. CAPT Sam DeBow, NOAA  
Hydrographic Survey Division  
Silver Spring, MD